



<b>Publication Year</b>	2020
<b>Acceptance in OA</b>	2022-02-11T11:47:40Z
<b>Title</b>	A kinematically unbiased, all-sky search for nearby, young, low-mass stars
<b>Authors</b>	Binks, Alexander S., Chalifour, Matthieu, Kastner, Joel H., Rodriguez, David, Murphy, Simon J., Principe, David A., Punzi, Kristina, SACCO, GIUSEPPE GERMANO, Hernández, Jesús
<b>Publisher's version (DOI)</b>	10.1093/mnras/stz3019
<b>Handle</b>	<a href="http://hdl.handle.net/20.500.12386/31388">http://hdl.handle.net/20.500.12386/31388</a>
<b>Journal</b>	MONTHLY NOTICES OF THE ROYAL ASTRONOMICAL SOCIETY
<b>Volume</b>	491

# A kinematically unbiased, all-sky search for nearby, young, low-mass stars

Alexander S. Binks<sup>1b</sup>,<sup>1,2★</sup> Matthieu Chalifour,<sup>3,4</sup> Joel H. Kastner,<sup>3</sup> David Rodriguez,<sup>5</sup> Simon J. Murphy<sup>1b</sup>,<sup>6</sup> David A. Principe,<sup>7</sup> Kristina Punzi,<sup>8</sup> Germano G. Sacco<sup>9</sup> and Jesús Hernández<sup>10</sup>

<sup>1</sup>*Astrophysics Group, Keele University, Keele, ST5 5BG, UK*

<sup>2</sup>*Instituto de Radioastronomía y Astrofísica, Universidad Nacional Autónoma de México (UNAM), Antigua Carretera a Pátzcuaro #8701 Ex-Hda. San José de la Huerta, Morelia, Michoacán, México. C.P. 58089*

<sup>3</sup>*Center for Imaging Science, 54 Lomb Memorial Drive, Rochester NY 14623, USA*

<sup>4</sup>*Physics & Astronomy Department, Swarthmore College, 500 College Avenue, Swarthmore, PA 19081-1397, USA*

<sup>5</sup>*Space Telescope Science Institute, 3700 San Martin Drive, Baltimore, MD 21218, USA*

<sup>6</sup>*School of Science, The University of New South Wales, Canberra, ACT 2600, Australia*

<sup>7</sup>*MIT Kavli Institute for Astrophysics and Space Research, 70 Vassar St, Cambridge, MA 02109, USA*

<sup>8</sup>*Astronomy Department, Wellesley College, 106 Central Street, Wellesley, MA 02481, USA*

<sup>9</sup>*Arcetri Observatory, 5, Largo Enrico Fermi, I-50125 Florence, Italy*

<sup>10</sup>*Instituto de Astronomía, UNAM, Unidad Académica en Ensenada, Ensenada 22860, México*

Accepted 2019 October 22. Received 2019 October 21; in original form 2019 February 7

## ABSTRACT

The past two decades have seen dramatic progress in our knowledge of the population of young stars of age  $< 200$  Myr that lie within 150 pc of the Sun. These nearby, young stars, most of which are found in loose, comoving groups, provide the opportunity to explore (among many other things) the dissolution of stellar clusters and their diffusion into the field star population. Here, we exploit the combination of astrometric and photometric data from *Gaia* and photometric data from GALEX (UV) and 2MASS (near-IR) in an attempt to identify additional nearby, young, late-type stars. Specifically, we present a sample of 146 GALEX UV-selected late-type (predominantly K-type) field stars with *Gaia*-based distances  $< 125$  pc (based on *Gaia* Data Release 1) that have isochronal ages  $< 80$  Myr even if equal-components binaries. We investigate the spectroscopic and kinematic properties of this sample. Despite their young isochronal ages, only  $\sim 10$  per cent of stars among this sample can be confidently associated with established nearby, young moving groups (MGs). These candidate MG members include five stars newly identified in this study. The vast majority of our sample of 146 nearby young star candidates have anomalous kinematics relative to the known MGs. These stars may hence represent a previously unrecognized population of young stars that has recently mixed into the older field star population. We discuss the implications and caveats of such a hypothesis – including the intriguing fact that, in addition to their non-young-star-like kinematics, the majority of the UV-selected, isochronally young field stars within 50 pc appear surprisingly X-ray faint.

**Key words:** stars: kinematics and dynamics – stars: late-type – stars: pre-main-sequence – solar neighbourhood.

## 1 INTRODUCTION

The identification and study of stars of age  $< 200$  Myr within  $\sim 100$  pc of the Sun provides crucial insight into pre-main-sequence (pre-MS) stellar evolution and the formative stages of planetary systems (Kastner 2016). Such young, nearby stars provide excellent samples for direct-imaging campaigns to observe exo-

planets, circumstellar discs and brown dwarfs (e.g. Kalas 2004; Lagrange et al. 2009; Bowler et al. 2015; Chauvin et al. 2015; MacGregor et al. 2015), act as direct observational test beds for early stellar evolution (e.g. Zuckerman & Song 2004; Bell, Mamajek & Naylor 2015), and provide key evidence for the physical origins of young stars in the solar neighbourhood and how they eventually disperse into the field population (e.g. Wright & Mamajek 2018).

The majority of these nearby, young stars can be placed in kinematically coherent ensembles known as nearby young moving groups (herein, MGs). To date, at least a dozen, and perhaps as many

\* E-mail: alex.s.binks@gmail.com

as two dozen, MGs have been identified (Mamajek 2016; Gagné et al. 2018). Their members are amongst the youngest stars known in the solar neighbourhood. These MGs are likely to have formed from the solar of more distant, dense star forming regions (Fernández, Figueras & Torra 2008), whose individual velocities are greater than the internal velocity dispersion, and subsequently escape in small groups. Since the ages for members of MGs can be resolved down to a few Myr, and MG member stars are approximately coeval (age spreads generally  $< 5$  Myr; Bell et al. 2015), any age determination methods for a star in an MG can reasonably be applied to any other star in the group; furthermore, age determinations from diverse methods can create a tight age constraint for the MG (e.g. Mamajek & Bell 2014). Recent work suggests that MGs share similar chemical abundances (Barenfeld et al. 2013; De Silva et al. 2013), which provides evidence for their common origins and hints at the compositions of the molecular clouds from which they were born.

Over the past two decades, the identification of candidate nearby, young, late-type stars and (hence) MG members among the field-star population has proceeded via some combination of their signature luminous chromospheric (UV) and coronal (X-ray) emission, which result from strong surface magnetic fields (e.g. Kastner et al. 1997; Rodriguez et al. 2013 and references therein), and their common Galactic ( $UVW$ ) space motions (e.g. Zuckerman & Song 2004; Torres et al. 2008; Malo et al. 2013). Follow-up spectroscopy then further constrains stellar ages via determinations of Li absorption line strengths, rotation rates, and optical activity indicators (such as  $H\alpha$  and the  $Ca\ II\ H + K$  lines and infrared triplet), so as to assess the viability of candidate MG stars or of proposed new MGs (see discussions in Zuckerman & Song 2004; Binks, Jeffries & Maxted 2015).

Because MGs are sparse and have spatial extents up to a few tens of pc (Gagné et al. 2018), their members can span wide areas on the celestial sphere. Hence, MG candidate selection has become increasingly reliant on kinematic and distance information, in addition to celestial coordinates and photometry. The fact that so many field stars, even within the nearest 100 pc, were missing parallaxes, precise proper motions, and/or radial velocity measurements presented a major difficulty for previous searches for MG candidates and tests of their membership status (e.g. Malo et al. 2014a). With the sudden availability of such data, in the form of the first two data releases from the *Gaia* space astrometry mission (Data Releases 1 and 2, hereafter DR1 and DR2; Gaia Collaboration 2016, 2018), the study of nearby, young stars and MGs can now make major strides. This potential motivated the recent study, described in Kastner et al. (2017), in which we evaluated the distances and ages of all 19 nearby young star candidates from the sample of  $\sim 2000$  stars compiled by the GALEX (UV, Bianchi et al. 2014) Nearby Young Star Survey (GALNYSS; Rodriguez et al. 2013) that were included in *Gaia* DR1. The youth of the majority of these 19 mid-K to early-M stars was supported by their positions, relative to both the loci of main-sequence (MS) stars and theoretical isochrones, in *Gaia* colour–magnitude and colour–colour diagrams. Surprisingly few of the GALNYSS stars included in *Gaia* DR1 have kinematics consistent with membership in known MGs, however (Kastner et al. 2017). Recent all-sky searches for nearby, young stars are beginning to identify dozens of new young stars unassociated with nearby MGs (Bowler et al. 2019; Schneider et al. 2019).

In this work, we further investigate the ability of *Gaia* to identify nearby, young stars and to assess their MG memberships – or lack thereof. Guided by the Kastner et al. (2017) study, we have used *Gaia* DR1 to select a sample consisting of a few hundred bright ( $7 < V < 12.5$ ) stars with GALEX UV counterparts that are isochronally young (ages  $\sim 80$  Myr). We then used DR2 data to assess these

stars’ kinematics. For subsamples of these *Gaia*/GALEX-selected nearby young star candidates, additional archival data (e.g. X-ray emission and Li absorption) have been compiled with which we can assess diagnostics of youth. Section 2 describes how the catalogue of 146 stars was generated, and Section 3 details how additional data were obtained from available literature sources and the spectroscopic observations that were acquired for a small subsample of the catalogue. Section 4 describes how Galactic kinematics were calculated as well as the kinematic tests used to test for MG membership. Results are presented in Section 5, focusing on stars that are new highly probable MG members and the majority of stars that have anomalous kinematics compared with known nearby MGs. In Section 6, we discuss the results and comment on specific areas where *Gaia* data have great potential to improve our understanding of young stars near the Sun. The results and conclusions are summarized in Section 7.

## 2 SELECTING CANDIDATE NEARBY, YOUNG STARS FROM GALEX AND GAIA DATA

This study was initiated before the release of DR2, and so relies entirely on DR1 for sample selection. However, for the analysis described in Section 4, we use DR2 astrometric and photometric data. This substitution is justified by the fact that, for our final sample of 146 objects, the absolute difference between DR1 and DR2 parallaxes is less than twice the combined error bar from DR1 and DR2 for  $> 95$  per cent of the sample stars, and this difference is never larger than 5.0 pc. Expanding on Kastner et al. (2017), our initial selection of stars for this study was based on cross-matching *Gaia* DR1 catalogue entries with the GALEX All-sky Imaging Survey (AIS) point source catalogue, but without the additional proper motion constraints used by Rodriguez et al. (2013).<sup>1</sup> We adopted a cross-matching radius of 3 arcsec to associate *Gaia* DR1 entries with NUV photometry from the GALEX AIS and, subsequently, near-IR ( $JHK_s$ ) and mid-IR ( $W1 - W4$ ) photometry from 2MASS and WISE, respectively, using the Vizier cross-match service.<sup>2</sup> This cross-matching exercise generated a catalogue with 715 773 objects.

We then selected stars within 125 pc (i.e. parallaxes  $\pi \geq 8$  mas) that lie significantly above the MS according to the models of Tognelli, Prada Moroni & Degl’Innocenti (2011, hereafter T11). Specifically, the T11 isochrones were used to select the subset of stars that appear younger than 80 Myr – even if equal-components binaries (see e.g. Kastner et al. 2017) – in an  $M_K$ , versus  $G - K_s$  colour–magnitude diagram (CMD; Fig. 1). The evolutionary models of Baraffe et al. (2015) and those of T11 agree to within a few tenths of a magnitude at 80 Myr for K- and early-M-type stars, with the T11 models consistently predicting older ages for low-mass stars (Kastner et al. 2017). For this reason, the T11 models are a more conservative choice for selecting stars younger than 80 Myr.

To further limit the sample size, we then selected only stars lying below (less luminous than) and redward of the T11  $1.0 M_\odot$  evolutionary track. No lower limit on mass was imposed, although the use of the Tycho catalogue to construct the DR1 catalogue imposes a magnitude limit of  $V \sim 12$ , which should result in a

<sup>1</sup> Here, as in Rodriguez et al. (2013), we select stars on the basis of presence of NUV photometry in the GALEX AIS catalogue, without regard to presence of FUV, because of the far more complete NUV coverage of the sky in the GALEX AIS data.

<sup>2</sup> <http://cdsxmatch.u-strasbg.fr/xmatch>

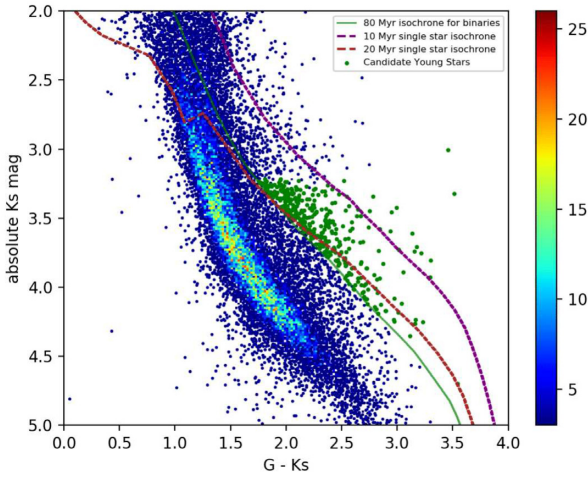


**Figure 1.** A  $K_s$  versus  $G - K_s$  colour–magnitude diagram (density plot) of GALEX UV-selected DR1 stars, with positions of 376 young star candidates indicated as green circles. Theoretical pre-MS isochrones from T11 for ages of 10 and 20 Myr as well as 80 Myr ‘binary stars’ are overlaid; i.e. the 80 Myr isochrone has been adjusted upwards by 0.75 mag, to simulate the positions of equal-components binaries of that age.

sample dominated by young K and early M dwarfs (see Section 3.2). Fig. 1 shows all of the *Gaia* DR1 and GALEX cross-matched stars, highlighting the 376 stars that we selected on the basis of lying above the 80 Myr equal-components binary isochrone and below and redward of the  $1.0 M_{\odot}$  pre-MS track.

Since chromospherically active stars can vary by several tenths of a magnitude in a given photometric band, and DR2 and 2MASS data are separated by observational baselines  $> 10$  yr, we further vetted the candidates that lie above the 80 Myr equal-mass binary isochrone in Fig. 1 via a CMD based purely on DR2 photometry. The resulting  $M_G$  versus  $G_{BP} - G_{RP}$  CMD is shown in Fig. 2, overlaid with isochrones for single and equal-mass binary stars of age 80 Myr and a 2 Gyr single-star isochrone to represent the MS (where these isochrones have been generated from the PARSEC 3.1 evolutionary models; Bressan et al. 2012).

Given the significant issues that have been raised by the astronomy community regarding the calibration of DR2 passbands with isochronal models (e.g. Gagné et al. 2018), we also compare our candidates with an empirical isochrone constructed for Pleiades cluster members (age =  $125 \pm 9$  Myr, Stauffer, Schultz & Kirkpatrick 1998; Melis et al. 2014). We collected DR2 photometry for 234 Pleiades candidates with  $G < 15$  that have  $> 99$  per cent membership probability in Olivares et al. (2018). To represent the single sequence for the Pleiades, we fit a quintic polynomial, removed all objects that lie  $> 0.25$  mag above the fit, and again fit with the same polynomial to the surviving members; the resulting sequence is represented by the green dashed curve in Fig. 2. Restricting candidates to those that lie above the empirical single-star Pleiades curve reduces the sample to 336 stars. The polynomial coefficients for the fit to the Pleiades single sequence are  $P_0 = 2.782$ ,  $P_1 = -6.598$ ,  $P_2 = 20.528$ ,  $P_3 = -16.178$ ,  $P_4 = 5.548$ , and  $P_5 = -0.708$ , with a dispersion in the fit  $\sim 0.020$  mag. Solid orange squares in Fig. 2 represent a sample of members in the  $\gamma$  Vel cluster (18–21 Myr, Jeffries 2014). The  $\gamma$  Vel sample are located in similar regions of the CMD as our target selection, confirming that our selected stars may be genuinely as young as  $\gamma$  Vel members. We further require that stars have a 2MASS  $K_s$  quality flag (Qflag) of value A, B, or C, and have artefact contamination (Cflag), extended source contamination (Xflag), and

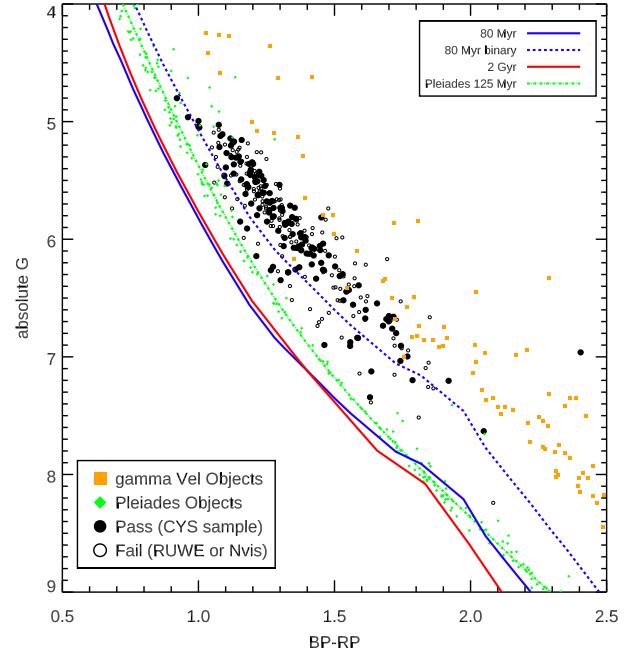


**Figure 2.** Absolute  $G$  versus  $G_{BP} - G_{RP}$  CMD, where open circles denote the 159 objects that satisfy all membership criteria except for the DR2 quality flags, and the other 146 objects that do satisfy these criteria – and, hence, constitute the final CYS sample – are displayed as black filled circles. Solid green diamonds and solid orange squares represent Pleiades (125 Myr) and  $\gamma$  Vel (18–21 Myr) members, respectively. The green dashed curve is the quintic polynomial used to describe the Pleiades single sequence. The red and blue solid lines map the 2 Gyr and 80 Myr PARSEC isochrones, respectively.

asteroid or comet association (Aflag) flags all set to zero, leaving 305 objects in the sample.

Finally, at the recommendation of the referee we employ a final requirement that all stars have at least eight DR2 visibility periods and for which the ‘renormalized unit weighted error’ (RUWE) is  $\leq 1.4$ , as suggested in Lindgren (2018), using the normalization factors provided by *Gaia*’s Data Processing and Analysis Consortium (DPAC). This cut helps filter contamination and astrometric effects from binary stars, and stars with poorly calibrated five-parameter astrometric solutions.

The foregoing selection criteria resulted in the sample of 146 stars that are highlighted in Fig. 2 as filled black circles and are listed in Table 1, and are herein referred to as the candidate young star (CYS) sample. These CYSSs are more or less uniformly distributed across the sky, with the exception of the GALEX Galactic plane avoidance zone. The candidate sample includes a small number of previously identified MG members (see Section 5.1) – including TW Hya, the namesake of the  $\sim 10$  Myr-old association whose identification spawned the wider search for MGs and their members (Kastner et al. 1997; Zuckerman & Song 2004; Torres et al. 2008). All object designations in the text are 2MASS identifiers and should be prefixed by ‘2MASS J’.

Both Figs 1 and 2 demonstrate that our CYS sample are clearly not well described by standard MS isochrones, in terms of their CMD positions, regardless of whether one refers to the theoretical or empirical (Pleiades) curves. It is furthermore apparent that the 159 stars that fail one or both DR2 quality flags (see above) occupy the same domain of *Gaia* CMD space (Fig. 2) as the 146 ‘survivors’. We comment further on the 159 ‘rejected’ stars in Section 6. We note

**Table 1.** The 2MASS identifier names, spectral types based on linear interpolation of  $G - K_s$  colour (SpTp), spectral types given in SIMBAD (SpTs), *Galex* NUV magnitudes, DR2 photometry, 2MASS K magnitudes, X-ray to bolometric luminosities, and UV excesses for the candidate young stars. The first 10 stars are listed here and the remaining stars can be accessed in the electronic version of this publication.

Name (2MASS J-)	SpTp	SpTs	NUV (mag)	G (mag)	G <sub>BP</sub> (mag)	G <sub>RP</sub> (mag)	K <sub>s</sub> (mag)	log( $f_x/f_{bol}$ )	$\Delta UV$ (mag)
00044817–4959504	K3.1		18.992 ± 0.056	10.8804	11.4445	10.1998	8.768 ± 0.021		+0.04
00092179+0038065	K4.0	K4Ve	18.290 ± 0.052	11.0253	11.6454	10.3281	8.711 ± 0.019	−3.21	−1.54
00475278–3245205	K3.7	K2Ve	16.696 ± 0.024	10.1600	10.7268	9.4748	7.899 ± 0.029	−3.10	−5.79
00524693+0948123	K1.6	K0	14.659 ± 0.008	8.3148	8.7536	7.7503	6.476 ± 0.027	−4.77	−0.76
01011333–4517578	K3.2	K0V	15.674 ± 0.012	9.6079	9.9796	8.9547	7.501 ± 0.026		−2.04
01445006–0805455	K1.3		17.260 ± 0.025	10.5147	10.9449	9.9450	8.703 ± 0.019		−0.34
01513522+0827126	K2.6		18.318 ± 0.055	10.5858	11.1220	9.9358	8.574 ± 0.021		+0.12
01524398–7445462	K3.1	K3V	16.531 ± 0.019	9.7562	10.3018	9.1044	7.675 ± 0.018	−3.58	−1.14
02115797+0421416	K4.7	K5	17.236 ± 0.017	9.4273	10.0699	8.7081	7.035 ± 0.026	−3.61	−1.25
02194778–3526443	K5.5	K2+Vk	15.109 ± 0.008	8.6211	9.0810	7.9023	6.084 ± 0.021	−5.02	−3.26

that use of DR2 instead of DR1 as the initial source of catalogued stars to be cross-matched with GALEX AIS would result in a sample of stars approximately a factor 9 larger than that listed in Table 1. Analysis of this far larger sample of  $\sim 1500$  stars is beyond the scope of this paper.

### 3 PROPERTIES OF THE CANDIDATE STARS

#### 3.1 Spectroscopic data

To assess the youth and evolutionary status of the CYSs closest to Earth, we obtained spectra for a small but presumably representative subsample of 24 stars in the brightness range  $7.5 < G < 11.6$  mag, the majority of which have distances  $d < 50$  pc. These 24 stars were randomly drawn from the sample of 305 stars that we compiled before application of DR2 data quality flags, since at the time of observing we had not enforced any DR2 quality criteria. 12 stars are among the ‘surviving’ CYS sample of 146 stars, and 12 are from the group of 159 that fail DR2 quality flag tests. This allows us to check on systematic differences between the spectra of DR2 data quality ‘rejects’ versus ‘survivors’.

Medium-resolution Echelle optical spectra ( $R \sim 18000$  at  $5000 \text{ \AA}$ ) were obtained for three candidate stars on four consecutive nights commencing 2017 June 30 using the Echelle spectrograph on the 2.1-m telescope at the San Pedro Mártir observatory (SPM), México. This instrumental set-up has a 2-pixel resolution of  $\sim 17 \text{ km s}^{-1}$ . Over 15 Echelle orders, the wavelength range of  $\lambda\lambda$  (4950–7000  $\text{\AA}$ ) easily covers the  $H\alpha$  and Li feature at 6562.8 and 6707.7  $\text{\AA}$ , respectively. An additional 12 stars were observed with the Wide-Field Spectrograph (WiFeS) on the Australian National University (ANU) 2.3-m telescope at Siding Spring Observatory ( $R \sim 7000$  at  $7000 \text{ \AA}$ , Dopita et al. 2007) over two consecutive nights commencing 2018 September 1, covering a wavelength range almost identical to the spectra obtained at SPM. Finally, 11 high-resolution spectra were obtained with the Magellan Inamori Kyocera Echelle on the Magellan telescope at the Las Campanas Observatory with  $1 \times 1$  binning, (MIKE;  $R \sim 65000$  in the red arm, using the 0.35 arcmin slit; Bernstein et al. 2003) on the night of 2019 March 24 with an average seeing of 0.45 arcsec. The MIKE spectrograph covers 34 Echelle orders between  $\sim 5000$ – $9000 \text{ \AA}$ , with a sampling units of  $0.05 \text{ \AA pixel}^{-1}$ .

We present our spectroscopically measured radial velocities (RVs),  $H\alpha$ , and Li equivalent widths (EWs) in Table 2, and heliocentrically corrected, normalized spectra centred around the  $H\alpha$  and Li line are presented in Fig. 3, where labels ‘R’ and

‘S’ correspond to either a rejection or a survival from the DR2 astrometric quality cuts, respectively. As noted, the representative spectroscopic sample were observed irrespective of their DR2 flag status, and we do not find any distinction between spectral characteristics of the ‘rejects’ and ‘survivors’. Only the 12 stars that survive the DR2 quality criteria are used for further analysis.

#### 3.1.1 Radial velocities

To avoid regions unsuitable for calculating RVs, the ANU long-slit spectra are separated into bins  $50 \text{ \AA}$  wide to simulate Echelle orders. For all spectra, relative RV shifts are calculated by fitting the cross-correlation function (CCF) using either a Gaussian (for narrow CCFs) or a parabola (for broad CCFs), and locating the pixel shift corresponding to the maximum height, using the IRAF program FXCOR (Tonry & Davis 1979). We measure the RV shift for each Echelle order and iteratively remove any outliers that are  $>2\sigma$  from the mean, avoiding orders that contain telluric contamination or very gravity-sensitive features. The final RV for all observations is weighted using the Tonry–Davis ‘R’ factor, which characterizes the height of the CCF peak compared to the full width at half-maximum.

For SPM and ANU observations, heliocentric RVs were calculated by cross-correlating the science spectra with RV template stars (observed on the same night and applying heliocentric velocity corrections to both the template and target star) within half a spectral type. For the MIKE spectra, the RV templates are replaced by synthetic spectra (Coelho et al. 2005) at solar metallicity and  $\alpha$ -enhanced chemical composition, degraded to the MIKE spectral resolution and signal to noise (SNR) over each Echelle order. The effective temperature ( $T_{\text{eff}}$ ) of the synthetic template chosen in each RV cross-correlation corresponds to the closest match in  $T_{\text{eff}}$  for the target star based on  $G - K_s$ . For SPM and ANU spectra, errors in RV are added in quadrature from three sources: (1) the error bar from the RV template, (2) the standard deviation in RV measurement across the spectral orders used in the cross-correlation, and (3) the error from cross-correlation of all RV templates on a given night. For MIKE spectra only error source 2 is used.

#### 3.1.2 Equivalent widths

We followed the same procedure in Binks et al. (2015) to measure  $H\alpha$  and Li EWs and uncertainties for the Li I line and corrected

**Table 2.** Subsample observed spectroscopically. Objects labelled with asterisks do not form part of the CYS sample because they did not satisfy the *Gaia* DR2 astrometric criteria. Spectral types are measured using the SPTCLASS software (Hernandez et al. 2017). SNR values for MIKE spectra are the interquartile range. Where no Li EW was observed the  $2\sigma$  upper limit is given.

Name (2MASS J-)	$G$ (mag)	$d$ (pc)	HJD (2450000-)	SpT	RV (km s <sup>-1</sup> )	SNR	Li EW (mÅ)	H $\alpha$ EW (Å)
San Pedro de Martır 2.1-m telescope – Echelle spectrograph								
0016+3031*	8.5088	39.276	7934.96117	K4.3	+2.02 $\pm$ 0.14	22	<56	+0.84
0052+0948	8.3148	44.982	7936.95071	K0.2		16	<78	+1.00
0211+0421	9.4273	46.825	7937.96785	K4.5	-65.36 $\pm$ 4.65	20	<62	+0.08
ANU telescope – WiFeS								
0052+0948	8.3148	44.982	8364.11052	G9.0	-0.9 $\pm$ 0.7	47	<26	+1.63
0211+0421	9.4273	46.825	8363.25773	K3.5	-57.3 $\pm$ 0.7	30	<42	+0.11
0219-3526 <sup>a</sup>	8.6211	34.870	8363.27311	K1.1	+2.1 $\pm$ 0.7	35	<36	+1.43
0235+1514*	9.2371	43.422	8363.27869	K3.5	-29.5 $\pm$ 0.6	27	<46	+0.76
					-76.8 $\pm$ 1.0	39	<32	
0341-7046	10.5656	44.101	8363.30671	K9.2	+1.5 $\pm$ 0.7	23	<54	+0.57
0341+0336*	8.9882	25.833	8363.24749	K2.6	+0.4 $\pm$ 0.8	21	<60	+0.56
0341-5125 <sup>b,*</sup>	8.6087	36.112	8363.31628	K3.5	+51.3 $\pm$ 0.7	39	<32	+0.86
2014-3936 <sup>c,*</sup>	11.2289	91.501	8364.12422	K6.0	-9.5 $\pm$ 1.0	30	<42	+0.74
2059-4758*	9.9843	42.495	8364.04859	K7.3	+3.9 $\pm$ 0.7	23	<54	+0.59
2142-3035*	9.9022	31.835	8364.05803	K5.5	+14.0 $\pm$ 0.6	24	<52	+0.60
2251-4646 <sup>d,*</sup>	9.1318	42.524	8364.07792	K1.0	-34.3 $\pm$ 0.7	37	<34	+1.09
2332-1215 <sup>e</sup>	9.8182	27.373	8364.11616	M0.6	+3.0 $\pm$ 0.8	17	152 $\pm$ 18	-1.83
Magellan telescope – MIKE Echelle spectrograph								
0950-2933 <sup>f</sup>	11.0389	121.068	8567.79963	K2.3	+14.10 $\pm$ 1.36	34-80	197 $\pm$ 4	-0.24
1018-3150	10.8465	65.644	8567.81306	K8.7	+15.74 $\pm$ 4.57	33-103	473 $\pm$ 4	-3.36
1037-0623*	9.4856	37.866	8567.80740	K9.1	-9.43 $\pm$ 0.24	36-104	<7	+0.71
1131-3436	10.4296	49.379	8567.79963	M0.4	+8.04 $\pm$ 1.47	33-173	547 $\pm$ 3	-14.89
1159-7601	10.8095	99.747	8567.89020	K5.2	+14.86 $\pm$ 0.30	41-111	429 $\pm$ 3	-0.21
1235-3452 <sup>f</sup>	7.4906	21.681	8567.83803	K1.9	-37.81 $\pm$ 0.27	72-170	<4	+0.87
1306-4609 <sup>*,b</sup>	11.6020	98.899	8567.88194	K3.2	+12.42 $\pm$ 2.41	23-74	<11	-2.78
1459-2406	11.2699	113.817	8567.91591	K4.9	-1.24 $\pm$ 0.31	38-94	314 $\pm$ 4	+0.08
1637+2919 <sup>f,g</sup>	11.0190	101.130	8567.79963	K5.2	-32.31 $\pm$ 0.74	32-102	<7	-0.66
					-48.82 $\pm$ 1.59			
1935-1502*	11.0877	104.858	8567.89839	K6.5	-5.73 $\pm$ 0.37	44-121	<6	+0.72
2032-4742*	10.0732	31.265	8567.91042	K8.0	-9.43 $\pm$ 0.18	36-116	<7	+0.62

*Note.* In this Table, and those that follow, for brevity we use only the first four characters in the right ascension and declination of 2MASS names; full designations are listed in column 1 of Table 1.

<sup>a</sup>VB, unresolved.

<sup>b</sup>Broad CCF, minimal asymmetry, SB?.

<sup>c</sup>nearby neighbour to the north west.

<sup>d</sup>VB, extracted both components (A = North).

<sup>e</sup>Known member of BPMG.

<sup>f</sup>double-lined CCF.

<sup>g</sup>RV resolved into two components.

for a blended Fe line at 6707.4 Å, by subtracting  $20(B - V) - 3$  mÅ, from the measured EW (Soderblom et al. 1993). The Li EW uncertainties are calculated using the formulation given by Cayrel de Strobel & Spite (1988). Where no Li line is apparent, or where the Li EW is found to be less than 40 mÅ, we quote  $2\sigma$  upper limits. For strong H $\alpha$  lines ( $>0.5$  Å) EW errors are assumed to be  $\sim 0.1$  Å. To identify any potential giants (or subgiants) in our spectroscopic sample, we assess the relative levels in the continuum around the Ca triplet (at 6102, 6122, 6162 Å), using the prescription in Prisinzano et al. (2012). We find no evidence that any of the stars in our own spectroscopic sample are giant stars.

### 3.2 Spectral types

We have assigned spectral types to the 146 CYSs by linearly interpolating  $G - K_s$  versus spectral type ( $G$  magnitudes all from

DR2) using the table provided by E. Mamajek.<sup>3</sup> We refer to these as photometric spectral types. For comparison, we find 69 stars with spectral types designated in the SIMBAD data base (Wenger et al. 2000). Fig. 4 shows that the majority of stars with spectral types available in SIMBAD (black filled circles) agree with the photometric spectral types to within half a spectral class, although we notice that SIMBAD spectral types are systematically approximately two spectral subclasses earlier than the photometric spectral types.

We find four examples in SIMBAD where the luminosity class is given as either a subgiant or giant. Two stars (labelled in Fig. 4) have SIMBAD spectral types  $\sim 2$  entire classes earlier than the photometric spectral types. Since both stars are within 100 pc, we do not expect this discrepancy to be due to reddening effects; rather,

<sup>3</sup>(herein EEM – <http://www.pas.rochester.edu/emamajek>).

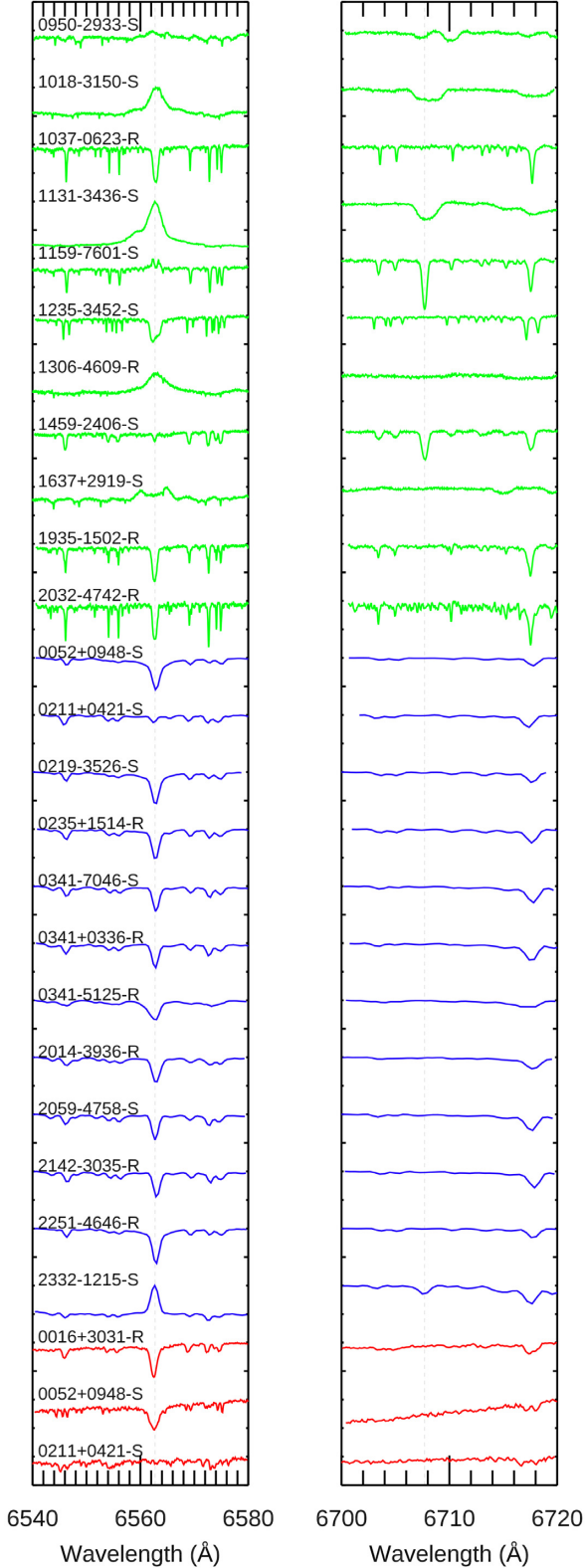


**Figure 3.** Spectra for the candidates observed at the SPM (red), ANU (blue), and MIKE (green) around the  $H\alpha$  feature at  $6563 \text{ \AA}$  (left) and the  $\text{Li I}$  feature at  $6708 \text{ \AA}$  (right). The name suffixes ‘S’ and ‘R’ indicate whether the star survives or is rejected from the CYS sample based on the DR2 astrometric criteria.

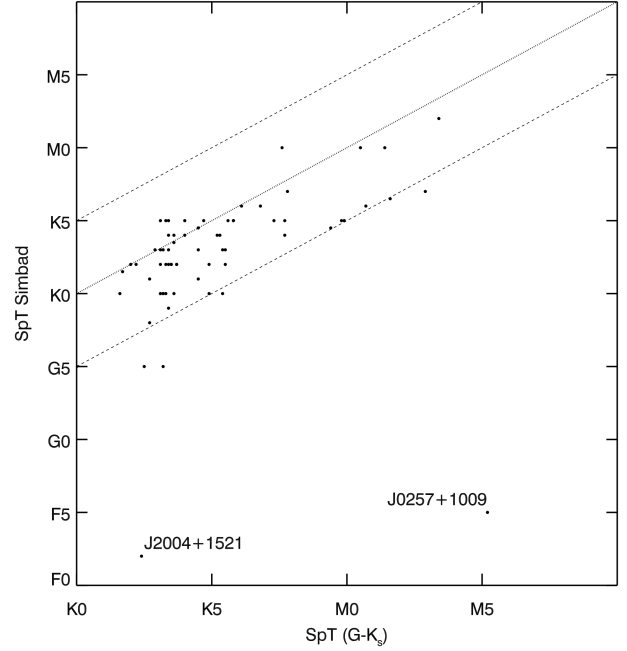


**Figure 4.** A comparison of SIMBAD spectral types with photometric spectral types. The solid line represents unity and the two dotted lines are deviations by half a spectral class.

it appears the SIMBAD source may not be correctly cross-matched with the DR2 source. As a cross-check, for our spectroscopic sample we find good agreement with the final spectral type adopted and those derived from our own spectral type analysis using the SPTCLASS code (Hernandez et al. 2017, listed in column 5 of Table 2).

As expected, the vast majority of the stars have K spectral types, a result of the combination of the range of  $G - K_s$  over which they were selected and *Gaia* DR1 magnitude limits (see Kastner et al. 2017). In total, the number of stars with spectral types G, K, and M are 5, 134, and 7, respectively. Spectral types and photometric magnitudes are listed in Table 1.

### 3.3 Age diagnostics

#### 3.3.1 *NUV* excess

Luminous UV is likely necessary but is clearly not sufficient to classify/identify a star as young; hence UV remains a good criterion for initial selection of young star candidates, as long it is subject to reasonable caution (and follow up). Kastner et al. (2017) demonstrated that UV-selected nearby young stars generally appear below the locus of MS stars in an  $NUV - G$  versus  $G - K_s$  colour-colour diagram, due to their enhanced levels of chromospheric activity and (hence) near-UV excesses. Fig. 5 confirms that the larger sample considered here adheres to this trend; the majority of the selected stars indeed lie below the MS locus. From the vertical distance between each CYS’s  $NUV - G$  and the main-sequence  $NUV - G$  versus  $G - K_s$  line (green line in Fig. 5), we obtain the estimated  $NUV$  excesses,  $\Delta NUV$ , that are listed in column 8 of Table 1. The fit used to provide the MS locus is  $NUV - G = 3.8(G - K_s) + 0.4$ .

In Fig. 6, we plot  $NUV - G$  versus isochronal age (and distance) for the 146 CYSs. For reference, we overplot the  $NUV - G$  means and  $1\sigma$  dispersions for K stars in the  $\beta$  Pic Moving Group (BPMG,

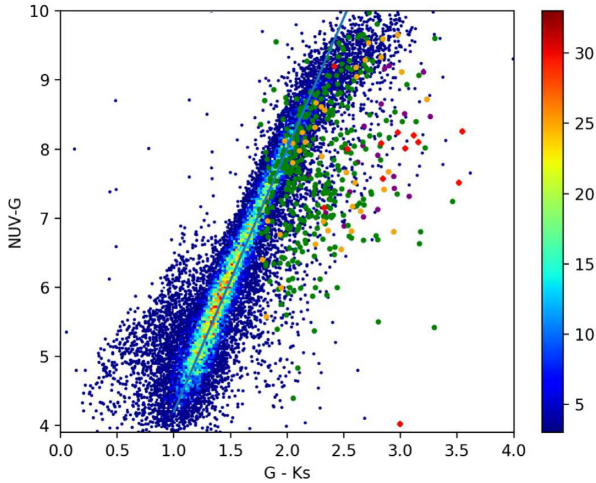


**Figure 5.**  $NUV - G$  versus  $G - K_s$  colour–colour diagram for all GALEX-selected stars in *Gaia* DR1, highlighting the same (376) initial DR1-selected candidates that are highlighted as green circles in Fig. 1 (green symbols; yellow symbols for stars within 50 pc) as well as the sample of (19) GALNYSS stars from Kastner et al. (2017, purple symbols), and previously identified nearby, young stars (red symbols). The green line indicates the locus of MS stars; the displacement of a star to the right of this line is indicative of the presence and strength of NUV excess.

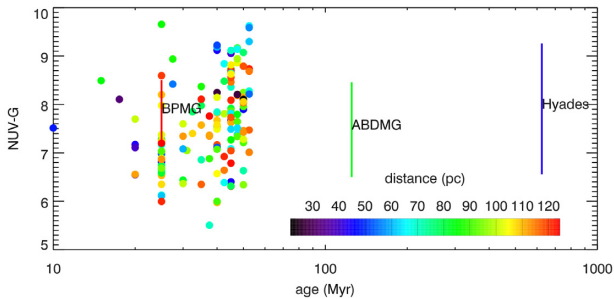


**Figure 6.**  $NUV - G$  versus isochronal age for the CYSSs, with the colour coding indicating distances to individual stars. The vertical line segments indicate the means and standard deviations of  $NUV - G$  for the  $\beta$  Pictoris MG (BPMG), AB Doradus MG (ABDMG), and Hyades.

age 21–26 Myr; Binks & Jeffries 2014; Malo et al. 2014b), AB Doradus Moving Group (ABDMG, age  $\sim 150$  Myr; Bell et al. 2015), and Hyades (age  $650 \pm 70$  Myr; Martín et al. 2018), which are measured as  $7.82 \pm 0.68$ ,  $7.48 \pm 0.98$ , and  $7.91 \pm 1.35$ , respectively. All three groups overlap within  $1\sigma$  of each other in  $NUV - G$ . Furthermore, the corresponding mean  $NUV - G$  for 217 K-type field-stars in the Gliese–Jahreiss catalogue (Gliese & Jahreiss 1991) is  $8.40 \pm 1.07$ , only slightly larger than (and within  $1\sigma$  of) the means of the presumably younger MG samples. While there is some separation of the two populations in Fig. 5, these statistics, along with Fig. 6, suggest that  $NUV - G$  (or, by extension, NUV excess) is of limited utility in isolating young K-type stars from the field population, which concurs with findings in Rodríguez et al. (2013).

### 3.3.2 X-ray emission

Strong X-ray emission in K stars is another potential indicator of stellar youth; it has long been recognized that pre-MS stars typically have measured values of  $\log L_X/L_{\text{bol}}$  in the range  $-4.0$  to  $-3.0$

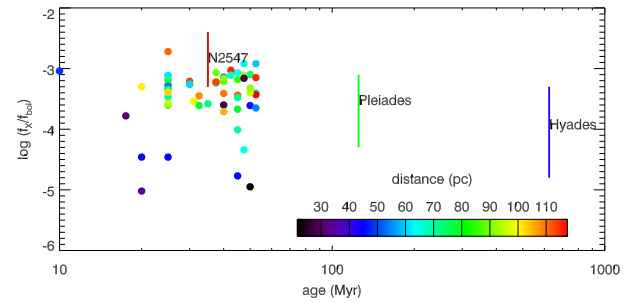


**Figure 7.** As in Fig. 6, but here we display  $\log f_X/f_{\text{bol}}$  ( $=\log L_X/L_{\text{bol}}$ ) versus isochronal age and distance for the candidate stars with RASS X-ray detections. The vertical line segments indicate the means and  $1\sigma$  dispersions of three young clusters.

(e.g. Kastner et al. 1997, 2017). Of the 146 CYSSs, we find 57 (39.0 per cent) that have *ROSAT* All-Sky Survey (RASS) X-ray count rates listed in either the 1RXP, 2RXS, or 2RXP catalogues (Voges et al. 1999, 2000; Boller et al. 2016).

RASS count rates were converted to  $f_X$  as described in Kastner et al. (2016), and bolometric fluxes ( $f_{\text{bol}}$ ) were estimated from the stars’ spectral types and  $J$  magnitudes using bolometric corrections listed in Pecaut & Mamajek (2013). The resulting plot of  $\log f_X/f_{\text{bol}}$  ( $=\log L_X/L_{\text{bol}}$ ) versus age (and distance) for the candidate stars with RASS X-ray detections is presented in Fig. 7, overlaid with the means and  $1\sigma$  dispersions in  $\log f_X/f_{\text{bol}}$  for K stars in three nearby young star clusters, NGC 2547 (age = 35 Myr; Jeffries & Oliveira 2005), Pleiades, and Hyades, to illustrate the temporal change in  $\log f_X/f_{\text{bol}}$  over the age range 35–650 Myr (see also Kastner et al. 1997). Comparison of Figs 6 and 7 provides tentative evidence that NUV emission remains elevated for K stars, even after X-ray emission begins to decline, and that both the X-ray and UV distributions may broaden after K stars arrive on the MS. These results are consistent with those of Stelzer et al. (2013), who found a similar relationship for UV and X-ray emission for M stars in MGs and in the field. The rather low overall RASS detection rate of the CYS – combined with the fact that the detections are dominated by the nearest stars, many of which have  $\log L_X/L_{\text{bol}} < -4.0$  (Fig. 7) – suggests that our CYS sample (Table 1) includes a significant number – perhaps a majority – of stars older than Pleiades age. We consider this possibility in detail in Section 6.1.

### 3.3.3 H $\alpha$ emission

The strength of H $\alpha$  emission provides another probe of stellar activity (Hawley et al. 1999; White & Basri 2003). It is well established that young, rapidly rotating, and (hence) active stars exhibit strong H $\alpha$  emission, which therefore also serves as an age indicator (Zuckerman & Song 2004). Measurements of H $\alpha$  in several open clusters of known age show that low-mass stars remain chromospherically active and retain H $\alpha$  in emission for longer than solar-type stars (Reid, Hawley & Mateo 1995), such that the utility of H $\alpha$  as an age diagnostic decreases with decreasing stellar mass.

Combining the results of our spectroscopic sample with a literature search using the VizieR data base, 41 stars among our final list of 146 CYS (28.1 per cent of the sample) are found to have at least one H $\alpha$  EW measurement, of which 22 are in emission. For 17 stars there are two or more separate H $\alpha$  EW measurements, from which we find broad agreement in every case and no stars with contradictory measurements between absorption and emission.

Our complementary spectroscopic survey (see Section 3.1 and Table 2) measured  $H\alpha$  EW for the first time in six stars. We list all  $H\alpha$  EW measurements and their reference sources in columns 3 and 4 of Table 3, respectively, where for stars with two or more  $H\alpha$  EW measurements the unweighted average is given. Individual  $H\alpha$  EW measurements and their references are available in a supplementary online table.

### 3.3.4 Infrared excesses

Evidence of either a transitional or debris disc, in the form of a mid-IR excess due to warm dust, is a potential youth indicator, as (with notable exceptions) such objects are mostly confined the age range  $\sim 10 - 100$  Myr (see e.g. Wyatt 2008; Matthews et al. 2014; Hughes, Duchêne & Matthews 2018). Various studies using photometry from the Wide-field Infrared Survey Explorer (*WISE*) have established that the general K/M field star population have *WISE*  $W1 - W4$  colours centred around  $W1 - W4 = 0$  with a dispersion of  $\sim 0.3$ , such that stars with  $W1 - W4 > 1.0$  are candidate debris disc hosts (e.g. Schneider, Melis & Song 2012; Binks & Jeffries 2017). There are two objects in our sample that have  $W1 - W4 > 1.0$  (and are labelled in Table 1): V1317 Tau (04234759+2940381), previously identified as a weak-lined T Tauri star associated with the Taurus cloud (Wichmann et al. 1996), and the intensively studied TW Hya (11015191–3442170; see Table 1), with  $W1 - W4 = 1.284$  and  $W1 - W4 = 5.585$ , respectively. Four Table 1 stars have moderate evidence of mid-/far-IR excess from Spitzer-based surveys: 1235–3452 (Lawler et al. 2009), 04392545+3332446, 11594226–7601260 (Wahhaj et al. 2010), and TW Hya (11315526–3436272 Rhee, Song & Zuckerman 2007).

### 3.3.5 Lithium absorption

Although theoretical models for Li depletion are strongly sensitive to surface conditions and stellar opacities, one can use empirical Li EW data in open clusters as benchmarks to distinguish stellar ages. There is a large dispersion in the Li EW distribution amongst K stars in young open clusters  $< 500$  Myr, which makes Li EW a useful age discriminant for stars of this spectral type. For stars with strong Li EW signatures ( $> 100$  mÅ), ages can potentially be resolved on the order of tens of Myr. We hence use these Li EW measurements to further constrain ages of the CYS sample.

39 of the CYSs have at least one Li  $\lambda 6708$  Å absorption line EW measurement, obtained either from literature sources or from our small spectroscopic survey (see Section 3.1). Our spectroscopic sample provides Li EW measurements for the first time in six stars, of which only 1459–2406 has a strong Li line ( $= 314 \pm 4$  mÅ). There are 11 stars that have two or more Li EW measurements, and for each of these stars the standard deviation in Li EW is always less than  $\sim 30$  mÅ.<sup>4</sup> For stars with two or more measurements, we calculate their unweighted average, which is used for all subsequent analyses. These values and the reference sources used to obtain this value are provided in column 5 and 6 of Table 3, respectively. All individual Li EW measurements are provided in an online supplementary table.

In Fig. 8, we plot Li EW against  $G_{BP} - G_{RP}$  colour for the 39 CYSs with Li measurements overlaid on the same data for members of  $\gamma$  Vel (age  $\sim 20$  Myr, Prisinzano et al. 2016), BPMG

**Table 3.**  $H\alpha$  and Li EW data.

Name (2MASS J-)	BP-RP (mag)	$H\alpha$ EW (Å)	Ref	LiEW (mÅ)	Ref	Li EW age (Myr)
0009+0038	1.3173	−0.2	a	100	a	~125
0047−3245	1.2520	−2.0	a	0	a	
0052+0948	1.0033	+1.315	*	<52	*	
0152−7445	1.1974			0	a	
0211+0421	1.3618	+0.095	*	52	*	
0219−3526	1.1787	+1.43	:	<36	:	
0339+6639	1.3296	+0.376	b	64	b	
0341−7046	1.6304	+0.57	:	<54	:	
0409+2901	1.1195	+0.95	cde	345	c	10–30
0423+2940	1.2618	−0.063	df			
0439+3332	1.5023	−0.7	dgh	495	i	10–30
0443−4106	1.1032	−0.2	a	<50	a	125–625
0450+2229	1.1730	+1.4	e	275	i	20–125
0452−1955	1.3066			190	j	~125
0500−5715	1.9194	−1.178	akl	340	ano	20–50
			m		p	
0521+2400	1.2219	−1.07	dq	380	dq	10–30
0641−5207	1.1771	+0.0	a	180	a	~125
0815+2946	1.1777	−0.158	r	20	r	
0833+3350	1.1589	+0.392	r	33	r	
0950−2933	1.2178	−0.22	a\$	249	a\$	20–125
0959+3849	1.2310	−0.694	r	<17	r	
1018−3150	1.7120	−3.32	aks	517	ano	10–30
			t\$		\$	
1101−3132	1.1925	+0.0	a	0	a	
1101−3442	1.6563	+166	akm	441	ano	10–30
			suv		s	
1131−3436	2.4045	−8.29	akm	553	ano	<20
			suv		sw\$	
			wx\$			
1133+3613	1.4580	−0.672	r	10	r	
1159−7601	1.4515	−0.417	agu	445	ajy	10–30
			y\$		\$	
1215−0237	1.7867	−1.037	kmz			
1221+2005	1.2243	+0.842	r	8	r	
1224−7503	1.3908	−0.4	a	0	a	
1235−3452	1.2734	+0.87	\$	<7	\$	
1459−2406	1.3168	+0.08	\$	314	\$	10–30
1637+2919	1.4156	−0.456	r\$	<7	r\$	
1757+5844	1.3975	−0.11	r	<11	r	
1916−5328	1.3442	+0.0	a	0	a	
2154+2239	1.7442	−0.70	m			
2223+3231	1.3776	+0.134	f			
2246−1759	1.1834	+0.0	a	160	a	~125
2252−6843	1.2510	+0.0	a	50	a	125–625
2259−4900	1.3777	−0.3	a	0	a	
2300−2618	1.7422	−0.1	u	15	ao	
2330−1717	1.1294	+0.0	a	30	a	125–625
2332−1215	2.0483	−1.66	akm	169	a:	20–125
			u:			

*Note.* References: a = Torres et al. (2006); b = Frasca et al. (2018); c = White, Gabor & Hillenbrand (2007); d = Kraus et al. (2017); e = Wichmann et al. (1996); f = Luo et al. (2015); g = Wahhaj et al. (2010); h = Alonso-Floriano et al. (2015); i = Wichmann et al. (2000); j = da Silva et al. (2009); k = Ansdell et al. (2015); l = Žerjal et al. (2017); m = Gaidos et al. (2014); n = Fernández et al. (2008); o = Mentuch et al. (2008); p = Yee & Jensen (2010); q = Li & Hu (1998); r = Binks et al. (2015); s = Schneider et al. (2012); t = Fang et al. (2017); u = Riaz, Gizis & Harvin (2006); v = Dent et al. (2013); w = Riedel et al. (2017); x = Riedel et al. (2018); y = Guenther et al. (2007); z = Schlieder, Lépine & Simon (2012); \* = SPM; : = ANU; \$ = MIKE.

<sup>4</sup>With the exception of 0950–2933 that has a standard deviation = 50 mÅ.

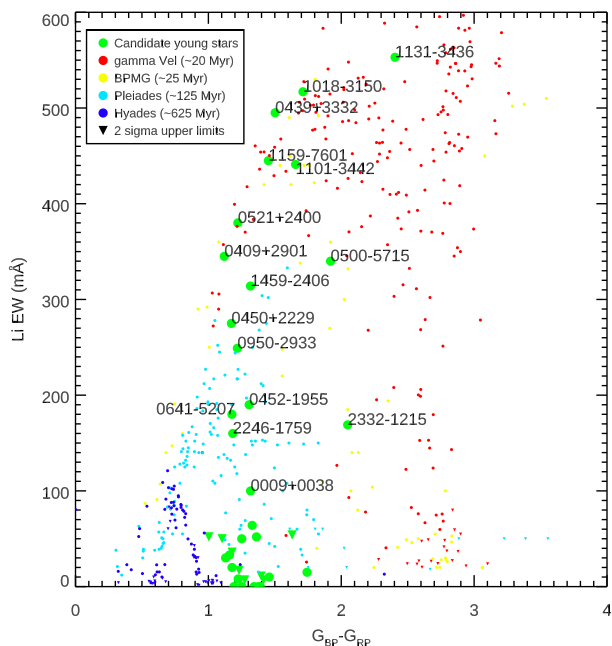


**Figure 8.** Plot of Li EW versus  $G_{BP} - G_{RP}$  colour for those CYs with available Li EW measurements (Table 3) and for various young clusters. Downwards facing triangles indicate  $2\sigma$  upper-limit measurements. The labelled targets have Li age upper-limits  $\leq 125$  Myr.

(age  $\sim 25$  Myr, Messina et al. 2016), Pleiades (Bouvier et al. 2018), and the Hyades (age  $\sim 625$  Myr, Cummings et al. 2017). This comparison suggests that 16 CYs have Li EW consistent with ages similar to the Pleiades, or younger, and nine of these are potentially younger than 50 Myr. Since the literature-sourced Li EW measurements are strongly biased towards stars likely to be members of young MGs, it is not surprising that the majority of Li detections in our sample of spectroscopically observed stars are previously established members of young MGs (see Section 5.3). The Li-absorption-based ages inferred from Fig. 8 are presented in column 6 of Table 3. Stars that have Li EWs consistent with Pleiades or younger ages are examined in more detail in Section 5.3.

## 4 KINEMATICS

### 4.1 Selecting radial velocities

The methodology of measuring RVs for our small spectroscopic sample is described in Section 3.1.1. To supplement these measurements, we performed a VizieR search for RVs for every member in our CYs sample. In total there are 102 stars (69.9 per cent) with at least one RV measurement (from our spectroscopic sample and/or the literature search), of which 27 have two or more measurements. Our spectroscopic sample measured an RV for the first time for four stars.

In some cases where an RV is reported in the literature, no error estimate is available. For these measurements we adopt a conservative error of  $3.0 \text{ km s}^{-1}$ , which is roughly twice the median uncertainty across all measurements with a published RV uncertainty. When applying our literature search, we identified a number of stars with two or more measurements that consist of large errors combined with small errors, which would potentially smear out hard-gained, high-resolution RV measurements. Therefore, we apply the following criteria: if the standard deviation amongst the

error bars is larger than the standard deviation in the mean then we elect the RV measurement with the lowest error bar. If the opposite is true, then we quote our final RV as the error-weighted mean, where the final error bar is the mean amongst the component errors. If the star is flagged as a probable binary based on large variability amongst individual RV measurements (see Section 4.2) then the final error bar provided is the quadrature sum of the standard deviation in the mean plus the final averaged error bar. All final RV measurements (and errors) and the source references used in each calculation are provided in columns 4 and 5 of Table 5, respectively. The individual RV measurements are provided in an online supplementary table.

### 4.2 Binarity

The unprecedented astrometric precision in DR2 allows us to identify probable common proper motion companions (CPMCs) that previously evaded detection in past surveys (e.g. the Washington Double Star Catalog). We apply a search radius of  $46.5 \text{ arcsec}$ . This is sufficiently wide to identify potential CPMCs out to projected separations from 2000 to 6000 au for our nearest and most distant CYs candidates, yet minimizes background star contaminants. This search yields 43 objects ( $\sim 30$  per cent of the CYs sample) with probable companions, i.e. stars with parallaxes within 3 per cent, and proper motions within 5 per cent, of a CYs.

We regard stars with CPMCs  $< 3 \text{ arcsec}$  as close pairs. Their proper motions may be indicative of orbital motion, however they may be prone to overlapping DR2 point spread functions (PSFs) that could distort the five-parameter astrometric solution (e.g. Kastner 2018). Slightly more than half of the stars with a CPMC (24 out of 43) are in close pairs, and the astrometric parameters may be prone to error. However, CPMCs separated by  $> 3 \text{ arcsec}$  should not be problematic for DR2. Since 2MASS PSFs are significantly lower resolution than the DR2 PSFs a number of stars will have resolved DR2 photometry, but unresolved in 2MASS, thus making them appear overluminous in a DR2/2MASS CMD ( $G$  versus  $G - K_s$ , Fig. 1). However, these stars would not appear overluminous in a ‘pure’ DR2-based CMD (see discussion in Section 6). The CPMCs are listed in Table 4.

Stars in multiple systems can vary significantly in RV, which complicates attempts to determine MG status from kinematics (see Section 4). We attempted to flag potential binaries by identifying those stars with two or more RV measurements that vary by an amount significant enough to suggest the variations are due to orbital motion. A scoring system was applied, based on the following metrics: a score of 0 represents a star with no RV measurements, whilst a score of 1 indicates a star with just one RV value. A score of 3 is given to stars with  $> 1$  measurement in which the absolute difference in the mean values of RV for all pairs is  $< 5 \text{ km s}^{-1}$ , and the quadrature sum of the error bars for every pair is  $< 5 \text{ km s}^{-1}$ , indicating that they are likely single stars. Stars that score 5 have  $> 1$  measurement, of which at least one pair is separated by  $> 5 \text{ km s}^{-1}$  and their errors (added in quadrature) is  $< 5 \text{ km s}^{-1}$ , such that the RV variability is indeed indicative of binary orbital motion. Finally stars with score 9 have  $> 1$  RV measurement, however, their error bars are too large to predict their binary status. We identify four objects in our CYs that are likely to be binary stars based on their RV variability; these four constitute  $\sim 15$  per cent of the sample with two or more RV measurements.

The object types that are provided in the SIMBAD data base were also used to indicate whether any objects are flagged as members of

**Table 4.** Stars with probable common proper motion companions in DR2, where column 2 describes the angular separation between the components. The first 10 stars are listed here and the remaining stars can be accessed in the electronic version of this publication.

Name (2MASS J-)	$r$ (as)	$\pi$ (mas)	$\mu_\alpha$ (mas yr <sup>-1</sup> )	$\mu_\delta$ (mas yr <sup>-1</sup> )	$G$ (mag)
0009+0038	15.6	9.2716 ± 0.0828 9.4633 ± 0.6243	+121.978 ± 0.120 +125.936 ± 1.099	-27.048 ± 0.097 -24.733 ± 0.711	11.0253 ± 0.0038 19.1824 ± 0.0044
0101-4517	0.5	14.1960 ± 0.0269 14.0202 ± 0.0420	+129.511 ± 0.034 +123.878 ± 0.062	+26.077 ± 0.036 +22.986 ± 0.049	9.6079 ± 0.0003 10.4047 ± 0.0009
0211+0421	20.3	21.3561 ± 0.0993 21.3649 ± 0.0519	-144.316 ± 0.121 -144.381 ± 0.075	-78.640 ± 0.154 -78.861 ± 0.072	9.4273 ± 0.0004 12.6154 ± 0.0003
0219-3526	1.9	28.6784 ± 0.0355 28.6758 ± 0.0394	-88.820 ± 0.030 -90.351 ± 0.036	+39.343 ± 0.049 +17.384 ± 0.061	8.6211 ± 0.0003 8.8098 ± 0.0003
0241-3735	0.3	11.7480 ± 0.0262 11.7587 ± 0.0359	+27.857 ± 0.030 +33.984 ± 0.039	-42.562 ± 0.042 -44.060 ± 0.081	11.7740 ± 0.0005 12.4029 ± 0.0005
0339+6639a	1.9	22.8417 ± 0.0312 22.8510 ± 0.0344	-79.635 ± 0.027 -74.190 ± 0.030	-21.683 ± 0.048 -8.488 ± 0.051	9.4879 ± 0.0004 9.8160 ± 0.0005
0339+6639b	1.9	22.8510 ± 0.0344 22.8417 ± 0.0312	-74.190 ± 0.030 -79.635 ± 0.027	-8.488 ± 0.051 -21.683 ± 0.048	9.8160 ± 0.0005 9.4879 ± 0.0004
0341-4516	1.2	8.0760 ± 0.0218 6.6154 ± 0.3144	+23.824 ± 0.034 +22.447 ± 0.672	-25.397 ± 0.042 -26.569 ± 0.688	11.5209 ± 0.0010 15.8465 ± 0.0092
0341-7046	9.7	22.6749 ± 0.0285 22.6765 ± 0.0437	+78.573 ± 0.050 +73.354 ± 0.083	+145.128 ± 0.058 +154.921 ± 0.088	10.5656 ± 0.0007 14.7510 ± 0.0006
0409+2901	6.8	9.0651 ± 0.0415 9.1769 ± 0.0435	+23.800 ± 0.093 +24.635 ± 0.093	-34.904 ± 0.046 -34.090 ± 0.050	10.4169 ± 0.0013 13.5890 ± 0.0009

**Table 5.** Kinematic data for the candidate young stars. The precision of the measurements are given to one decimal place, however, are generally more precise. The first 10 stars are listed here and the remaining stars can be accessed in the electronic version of this publication, where their full precision values are quoted.

Name (2MASS J-)	$\mu_\alpha$ (mas yr <sup>-1</sup> )	$\mu_\delta$ (mas yr <sup>-1</sup> )	RV (km s <sup>-1</sup> )	Flags	$\pi$ (mas)	$U$ (km s <sup>-1</sup> )	$V$ (km s <sup>-1</sup> )	$W$ (km s <sup>-1</sup> )
0004-4959	+190.6 ± 0.3	-24.3 ± 0.6	-55.2 ± 1.3	a,1	8.7 ± 0.3	-104.9 ± 0.7	-44.6 ± 0.4	+36.2 ± 1.2
0009+0038	+124.1 ± 3.5	-26.8 ± 1.5	-31.9 ± 5.8	a,1	8.9 ± 0.9	-44.6 ± 0.8	-54.7 ± 2.8	+11.1 ± 5.1
0047-3245	+246.9 ± 0.2	-11.9 ± 0.1	+1.0 ± 3.0	b,1	13.7 ± 0.3	-69.5 ± 0.3	-49.3 ± 0.2	-1.8 ± 1.0
0052+0948	-33.4 ± 0.1	-49.4 ± 0.1	-0.9 ± 0.7	:,1,**	22.6 ± 0.3	+10.9 ± 0.2	-3.6 ± 0.4	-5.7 ± 0.6
0101-4517	+129.6 ± 0.1	+25.7 ± 0.1	-15.3 ± 0.4	b,1,**	14.6 ± 0.3	-41.1 ± 0.1	-13.1 ± 0.1	+13.7 ± 0.4
0144-0805	-37.2 ± 2.6	-50.0 ± 1.0	+22.907 ± 1.035	ac,3	8.1 ± 0.6	+27.1 ± 0.4	-2.4 ± 0.2	-35.9 ± 1.0
0151+0827	+38.6 ± 2.1	+9.4 ± 0.6	+36.85 ± 0.36	c,1	9.0 ± 0.3	-36.2 ± 0.2	+3.5 ± 0.1	-21.3 ± 0.3
0152-7445	+61.9 ± 1.1	+83.5 ± 0.8	+6.778 ± 2.853	a,1,WUMa	13.8 ± 0.2	-31.5 ± 1.0	-5.4 ± 1.9	-21.2 ± 1.9
0211+0421	-144.4 ± 0.1	-78.9 ± 0.1	-57.479 ± 6.296	*,5	21.7 ± 0.2	+62.3 ± 3.5	-5.3 ± 1.4	+27.0 ± 5.0
0219-3526	-87.0 ± 0.1	+39.9 ± 0.1	+1.593 ± 0.500	b:,3	28.1 ± 0.3	+5.2 ± 0.1	+13.5 ± 0.2	-7.1 ± 0.5

*Note.* RV references: a = Kunder et al. (2017); b = Gontcharov (2006); c = Gaia Collaboration (2018); d = Frasca et al. (2018); e = Nguyen et al. (2012); f = Barbier-Brossat, Petit & Figon (1994); g = Malaroda et al. (2000); h = Torres et al. (2006); i = Elliott et al. (2014); j = Montes et al. (2001); k = Murphy, Lawson & Bessell (2013); l = Duflot, Figon & Meyssonnier (1995); m = Schlieder, Lépine & Simon (2010); n = Sperauskas et al. (2016); o = Malo et al. (2014a); \* = measured from spectrum collected at the SPM; : = measured from spectrum collected at the ANU. Binary flags: 0 = no RV measurements, binary status is indeterminate; 1 = 1 RV measurement, binary status is indeterminate; 3 = >2 RV measurements, all of which are within 5 km s<sup>-1</sup> of one another and their errors (added in quadrature) are < 5 km s<sup>-1</sup> and are likely single stars; 5 = >2 RV measurements, of which at least one pair are separated by > 5 km s<sup>-1</sup> of one another and their errors (added in quadrature) are < 5 km s<sup>-1</sup> and are likely to be binary stars; 9 = errors are too large to determine their binary status. Simbad flags are: \*\* = double star; BYDra = BY Draconis; WUMa = eclipsing binary star of type W Ursa Majoris; EB\* = eclipsing binary; SB\* = spectroscopic binary star; RSCVn = RS Canum Venaticorum variable star; Algol = eclipsing binary of Algol type;  $\beta$ Lyr = eclipsing binary of  $\beta$  Lyrae type.

multiple systems. In total there are 55 stars (38 per cent of the CYS) that display evidence of binarity, either based on DR2 companions, our binary scoring, or SIMBAD indication (37.7 per cent of the CYSs). The multiplicity fraction for our predominantly K-star sample fits entirely in the progression observed in volume-limited stellar multiplicity samples of both G-dwarfs (44 ± 3 per cent, Raghavan et al. 2010) and early M-dwarfs (31.1 ± 3.4 per cent, section 6.1 in Winters et al. 2019). It is entirely possible that our search may miss potential MG candidates among these 55 stars, or provide false positives, because of RV variation due to binarity. The binary scores used in this work and any evidence pertaining to binary stars from SIMBAD are presented in column 5 of Table 5.

We briefly discuss the binary status for stars of notable interest in Section 5.

### 4.3 Determining UVW space velocities

Galactic space velocities ( $UVW$ ) and their errors are calculated using positions, proper motions, RVs, and parallaxes (and their associated errors) following the prescription in Johnson & Soderblom (1987). All 146 *Gaia* DR1-selected objects in our CYS sample have position, proper motion, and parallax data available in the DR2 catalogue. The median errors are 0.0411 mas, 0.0847 mas yr<sup>-1</sup>, and 0.0400 mas, respectively, where the positional and proper motion

errors are the quadrature sum of the error components in right ascension and declination. Since the parallax SNR ratios are never  $< 10$  we simply treat distances as the parallax inverse.

For the 44 stars that have no RV measurement,  $UVW$  are calculated over a range of  $-100 < RV(\text{km s}^{-1}) < +100$  in steps of  $0.5 \text{ km s}^{-1}$ . The  $UVW$  for each star are listed in columns 7, 8, and 9 of Table 5, where the  $UVW$  for stars without an RV are displayed by their extrema from the RV range. Fig. 9 depicts the  $UVW$  distribution for the stars with RV measurements, with the  $1\sigma$  extents of 11 well-known nearby MGs overplotted ( $UVW$  means and  $1\sigma$  dispersions are taken from the covariance diagonals quoted in table 7 of Gagné et al. 2018).

#### 4.4 Kinematic tests for MG membership

Measuring Galactic kinematics and comparing to those of known young MGs is the one of the primary methods to confirm the youth of CYSs and to test their memberships in MGs. If a CYS appears to be comoving with a known MG, it is a potential member and could therefore have an age co-eval with the proposed host group. To establish whether there exists a subset of our 146 candidate stars that are possible or established MG members, we applied the following four kinematic and distance-based membership tests.

(i) A  $\chi_{\text{MG}}^2$  test, as described in Shkolnik et al. (2011) and Binks et al. (2015), where  $\chi_{\text{MG}}^2$  is defined as

$$\frac{(U_* - U_{\text{MG}})^2}{\sigma_{U_*}^2 + \sigma_{U_{\text{MG}}}^2} + \frac{(V_* - V_{\text{MG}})^2}{\sigma_{V_*}^2 + \sigma_{V_{\text{MG}}}^2} + \frac{(W_* - W_{\text{MG}})^2}{\sigma_{W_*}^2 + \sigma_{W_{\text{MG}}}^2}$$

and is required to be  $\leq 3.78$ . Such a threshold rejects the null hypothesis with 95 per cent confidence. The  $UVW$  data for MGs used in this analysis are from table 7 of Gagné et al. (2018).

(ii) A kinematic distance test comparing the measured distance and the expected distance if the object were a member of the cluster, in which the difference between the measured distance and the expected distance must be less than 10 pc.

(iii) The star must have an RV measurement within  $5 \text{ km s}^{-1}$  of the expected RV were it a member of a given MG.

(iv) The star must have a mean distance measurement within the  $3\sigma$  dispersion of the proposed MG, where the mean distance and  $1\sigma$  dispersions are the quadrature sums of  $XYZ$  and their dispersions from table 7 of Gagné et al. (2018).

These criteria are applicable for *all* objects with an RV measurement in the CYS list, and for stars without RV measurement all criteria except for the RV test can be applied.

We tested a reasonable range of RVs for the stars in the CYS sample that have no measured RV, and found that one of them, 2223+3231, could be within  $\chi_{\text{MG}}^2 \leq 3.78$  of an MG if the actual RV lies within a small range given in Table 6. In addition to the kinematic criteria, one must ensure that the measured age of the star is at least consistent with the age range of the proposed host MG. Individual stars will be discussed in the following section.

## 5 RESULTS

### 5.1 Candidate MG members

After applying the criteria described in Section 4.4, we find a subset ( $\sim 15$  per cent) of CYSs that are potential MG members, based on either our kinematic criteria, previous membership assignments in the literature, or both. In this section, we assess the evidence for MG

membership based on data collected in this work, or from previous literature, and provide our diagnosis for each object.

In Table 6, we list the 21 potential MGs members identified among the 146 CYSs. The table is split into three sections. For each candidate MG member we utilize the BANYAN $\Sigma$ <sup>5</sup> probability code, which calculates the probabilities of membership in 29 young associations within 150 pc of the Sun based exclusively on astrometric and kinematic data.

All MGs for which BANYAN $\Sigma$  membership probabilities are  $> 10$  per cent are listed in column 10. We adopt such a low BANYAN $\Sigma$  probability threshold so as to attempt to identify new candidate MG members that could lie in tails of the probability  $UVW$  distributions, and also because we do not strictly employ the  $XYZ$  positions as a membership criterion. The top two sections list stars that pass all appropriate kinematic membership criteria in Section 4.4 with reference to any of the 11 MGs considered in this work. There are 13 stars with an RV measurement in the top section of Table 6, and one star without a measured RV in the middle section of the Table. The membership status of this star is more ambiguous because it requires an RV measurement within the range quoted in column 5 to pass the RV criterion from Section 4.4.

The bottom section of Table 6 lists data for seven stars that have evidence for MG membership, either from literature sources or a BANYAN $\Sigma$  membership probability  $> 10$  per cent, but fail the  $\chi_{\text{MG}}^2$  criterion. The fact that previous MG searches identified some of our candidates as members that our selection criteria omitted, and vice versa, presumably reflects the way membership criteria are defined, the  $UVW$  velocity distributions used for given MGs, and/or the different data sets used in the selection process. We finally note that, although none of the following objects in this section were revealed to be binaries based on RV variation, binarity may none the less affect the kinematics of *any* star in this work.

In the following, we briefly discuss relevant factors regarding MG membership status for each star in Table 6 and provide our assessment of the most likely MG membership (if any), beginning with objects in the top section of the Table (the abbreviated forms for each MG are listed in the table notes at the bottom of Table 6). The final designated membership status for each object is provided in the final column of Table 6.

#### 5.1.1 Stars with a measured RV that pass all kinematic criteria

The following seven stars satisfy all kinematic criteria for membership to a given MG, and there is either literature pertaining to MG membership and/or a BANYAN $\Sigma$  probability  $> 10$  per cent for the same proposed group.

**05004714–5715255:** There is a kinematic match to both BPM and TWA, although the match with BPM is much better in each membership criterion, and its sky position is inconsistent with TWA membership. There are both many listings for this star as a BPM member in the literature and a near-unity probability predicted from BANYAN $\Sigma$ . The Li EW measurement is in agreement with the pattern observed amongst similar spectral type BPM members, thus we confirm its status as a member of BPM.

**10182870–3150029:** There are two kinematic matches, which are COL and TWA. Whilst previous literature suggests this target is a TWA member, the kinematic match in our analysis is better for COL. The Li EW measurement agrees with both MGs, albeit only

<sup>5</sup>available at <http://www.exoplanetes.umontreal.ca/banyan>.

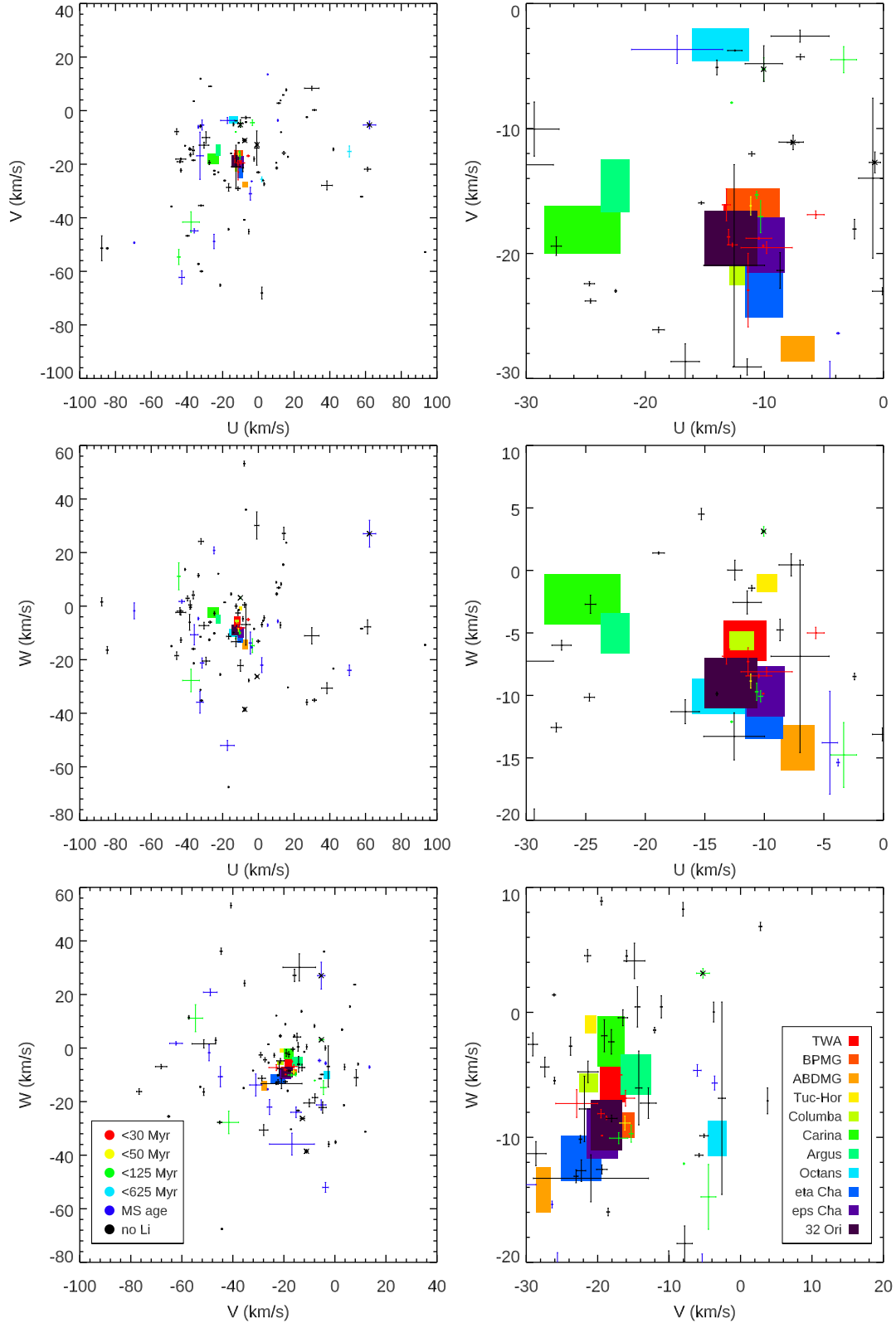


**Figure 9.** *UVW* space velocities of the 102 nearby young star candidates with an RV measurement, along with the  $1\sigma$  ranges of 11 well-established MGs (Binks, Jeffries & Ward 2018) indicated. The left-hand panels encompass the *UVW* range of the entire sample, whereas the right-hand panels provide zoomed-in views of the MG centroids.

**Table 6.** Candidate MG members.

Name (2MASS J-)	Age (Myr)	Distance (pc)	Kinematic match(es)	$t_1$	$t_2$ (pc)	$t_3$ (km s <sup>-1</sup> )	$t_4$	MG <sub>lit</sub>	BANYAN	Final choice
Stars with a measured RV and pass all kinematic criteria.										
0409+2901	10–30*	110.313	THO	1.22	−0.25	−0.87	0.54		TAU(13.7)	TAU
			COL	3.60	−8.02	+1.46	0.76			
0439+3332	10–30*	90.092	THO	0.69	−0.20	−3.18	0.18			TAU
			EPS	0.47	−1.42	−0.38	0.67			
			TWA	2.39	+7.79	−1.69	0.76			
0500–5715	20–50*	26.901	BPM	0.03	+0.75	+0.08	0.09	BPM <sup>abcd</sup>	BPM(99.9)	BPM
			TWA	2.78	−4.91	+0.59	0.60			
0521+2400		88.267	THO	0.58	−0.28	−2.39	0.24		118(99.8)	118
			EPS	0.44	−4.40	+0.39	0.78			
			TWA	3.04	+7.70	−0.75	0.72			
0950–2933	20–125*	121.068	THO	1.53	−5.84	−2.30	0.91			YFS
1018–3150	10–30*	65.644	COL	1.15	+4.58	+0.96	0.29	TWA <sup>ab</sup>		TWA
			TWA	1.53	+8.38	+4.10	0.23			/COL
1101–3442	10–30*	60.086	COL	3.24	+0.72	−2.78	0.23	TWA <sup>abcd</sup>	TWA(99.9)	TWA
			TWA	0.79	+5.18	+0.23	0.12			
1121–4736	<10–40	70.723	THO	1.26	+9.09	+1.15	0.86			IFS
			ABD	2.42	+0.55	−7.56	0.58			
1131–3436	<20	49.379	BPM	2.51	+1.03	+0.48	0.32	TWA <sup>abcd</sup>		TWA
			TWA	1.21	+2.45	−2.48	0.12			
1159–7601	10–30*	99.747	THO	1.67	−9.20	+2.01	0.16	CAR <sup>d</sup>	EPS(99.9)	EPS
			EPS	0.02	+1.32	+0.02	0.11			
1215–0237	10–60	51.590	ABD	2.76	+3.41	+2.42	0.39		ABD(19.7)	ABD
2135+3402	15–60	75.764	OCT	0.96	+0.76	−1.84	0.15			OCT
2332–1215	20–125*	27.373	BPM	0.41	−0.49	+0.94	0.10	BPM <sup>abc</sup>	BPM(99.9)	BPM
One star without a measured RV, with $\chi^2 < 3.78$ for <i>some</i> RV configuration and pass all other kinematic criteria.										
2223+3231		85.497	OCT		−9.25		0.11			OCT
				8.5,12.5						
Stars classed as MG members in literature, missed in our search										
0405–0216	25–80	40.289					0.62		HYA(48.9)	HYA
0418+2317	10–60	54.008					0.12		HYA(96.5)	HYA
0450+2229	20–125*	123.684					0.11		TAU(99.8)	TAU
0452–1955	~125*	61.686	THA(74.23)		−14.39	+43.77	0.29	THA <sup>c</sup>		YFS
1459–2406	10–30	113.817					0.13		UCL(94.6)	UCL
							0.29		USC(0.3)	
2213+8445		61.523			+0.27		0.37		ARG(66.3)	IFS
2300–2618	10–60	31.859	ABD(6.63)		+1.75	+2.56	0.19		ABD(96.7)	ABD

*Note.* All candidate young stars that have some kinematic match to a known MG, either from our analyses, has a candidate or member status from a literature source, or both. Columns  $t_{1-4}$  are the results of the kinematic criteria described in Section 4.4. Top section: objects with at least one RV measurement and satisfy all kinematic criteria given in Section 4.4. Middle section: objects that lack any RV measurement but would have some RV value satisfying the  $\chi^2$ -test. We provide the RV range corresponding to an  $\chi^2$ -test success in the  $\chi^2$  column. Bottom section: objects that fail the  $\chi^2$  test, however are identified as MG members either as candidate MG members in the literature and/or with probabilities >10 per cent for a given MG based on the BANYAN  $\Sigma$  code. If the potential host MG suggested in the literature is one of the 11 MGs analysed in this work, then the  $\chi^2$  value (always >3.78) is provided in the  $\chi^2$  column. The abbreviations used for the groups in this work are as follows: ABD = AB Doradus, ARG = Argus, BPM =  $\beta$  Pictoris, COL = Columba, EPS =  $\epsilon$  Cha, ETA =  $\eta$  Cha, HYA = Hyades, LCC = Lower Centaurus Crux, OCT = Octans, TAU = Taurus, THA = Tucana Horologium, THO = 32 Ori, TWA = TW Hya, UCL = Upper Centaurus Lupus, USC = Upper Scorpius. Ages with superscripted asterisks are those measured using Li EWs (see Table 3 and Fig. 8 for reference). Final designations YFS and IFS are ‘young field stars’ and ‘indeterminate-age field star’, respectively. Note that 1018–3150 is also a possible member of COL.

<sup>a</sup>Malo et al. (2013).

<sup>b</sup>Bell et al. (2015).

<sup>c</sup>Zuckerman & Song (2004).

<sup>d</sup>Torres et al. (2008).

marginally with COL. We therefore cannot discriminate between the two potential host MGs (if indeed there is one) and designate the star as a possible member of TWA or COL.

**11015191–3442170:** This object is TW Hya, the eponymous TWA member (Kastner et al. 1997).

**11315526–3436272:** Identified as TWA 5, this object is another of the original five members of the TWA (Kastner et al. 1997) and,

hence, also serves as confirmation of our young-star candidate selection and MG membership methodologies. Specifically, we have two kinematic matches (to TWA and BPM) but TWA provides the best  $\chi^2$  match and BANYAN $\Sigma$  predicts a 99.9 per cent membership probability to TWA. The strong Li EW line suggests the star’s age <20 Myr, consistent with stars of similar spectral type that have subsequently been identified as TWA members.

**11594226–7601260:** Whilst there are two kinematic matches, to EPS and THO, the best  $\chi^2$  match, by far is to EPS, and has previously been categorized numerous times as an EPS member since the original designation by Mamajek, Lawson & Feigelson (2000). The BANYAN $\Sigma$  code predicts a 99.9 per cent membership probability to EPS, and the measured Li EW is consistent with this membership. We therefore (re)assign this star as most likely a member of EPS.

**12151838–0237283:** There is one single kinematic match with ABD, and several literature sources suggest it as a candidate ABD member. There is a corresponding 19.7 per cent BANYAN $\Sigma$  membership probability. Whilst there is no Li EW measurement available for this star, it has relatively strong X-ray activity ( $\log f_X/f_{\text{bol}} = -3.65$ ), notionally consistent with stars of ABD age. We suggest that this star requires further analysis, particularly a Li EW measurement. We concur with previous work and propose this star as a candidate member of ABD.

**23323085–1215513:** This object has been identified several times as a bonafide member of BPM. We find only one kinematic match, which is also with BPM, and the BANYAN $\Sigma$  code provides a corresponding membership probability of 99.9 per cent. The final Li EW measurement, which includes one measurement obtained in this work is consistent with membership, therefore we confirm its status as a member of BPM.

The following two stars, also listed in the top section of Table 6, have membership assignments in literature sources that do not match with ours.

**04090973+2901306:** We find a potential match with THO or COL. The sky position of this star place it outside the region of sky occupied by most known THO members. It is also likely too distant to be a COL member. There are several literature sources that claim the object is a member of TAU. Despite the low BANYAN $\Sigma$  membership probability for TAU of 13.7 per cent, the distance, sky position, and Li EW are all consistent with constituents in TAU. We conclude that this object is indeed most likely a member of TAU.

**05214684+2400444:** This objects passes all kinematic criteria for both THO and EPS, whilst BANYAN $\Sigma$  predicts an almost unity probability of membership to 118TAU. The large Li EW suggests the star is  $<30$  Myr, consistent with all three groups. The sky position definitively rules out membership with EPS, and membership to THO is marginally ruled out as the target is  $\sim 5^\circ$  further north than the most northerly THO members in Bell, Murphy & Mamajek (2017), whereas it is very close to the centroid of 118TAU. We therefore assign this object as a member of 118TAU, which agrees with the recent designation by Bowler et al. (2019).

Finally, the following four objects listed in the top section of Table 6 have no previous evidence of MG membership in the literature or any BANYAN $\Sigma$  probabilities  $>10$  per cent.

**04392545+3332446:** There are kinematic matches to EPS, THO, and TWA, and a strong Li EW measurement and strong X-ray activity, and short rotation period ( $=2.418$  d, Watson, Henden & Price 2006) are consistent with the young ages for each of these MGs. However, the sky position conclusively rules out membership in any of these groups. Several publications posit that the star is a member of TAU, despite a BANYAN $\Sigma$  of only 0.1 per cent. The largest difference in velocity is in the  $V$  coordinate, both in standard deviations ( $2.04\sigma$ ) and numerically ( $|\Delta V| = 10.2 \text{ km s}^{-1}$ ). Given the lack of alternative MGs, we tentatively designate this object as a member of TAU.

**09503676–2933278:** We find a kinematic match with THO. The measured Li EW is consistent with membership, while the

sky position is inconsistent. There are no literature sources found pertaining to a membership status, despite its inclusion in the catalogue input to the SACY search (Torres et al. 2006). For present purposes, we classify this star as a young field star.

**11212188–4736028:** Whilst we find a kinematic match with THO, the sky position is inconsistent with the group. The object is a K2 III + K2 III eclipsing binary, which may describe the star's overluminosity compared to the CMD MS (as opposed to youth). We assign the membership status as an indeterminate field star.

**21351099+3402313:** Only one kinematic match is found, with OCT. There are no literature references to this target, and no specific additional youth evidence. We tentatively suggest this object as a potential member of OCT.

### 5.1.2 One star without a measured RV

**22233510+3231182:** There is a potential match with OCT for this object, and coincides with the required distance for membership. No literature references are found for this source. One measurement of H $\alpha$  is found in absorption and no additional youth indicators were identified. Thus we suggest this star is a potential member of OCT, pending spectroscopic confirmation.

### 5.1.3 Stars classed as MG members in literature, missed in our search

Finally, there are seven stars listed in Table 6 (bottom section) that have previously been assigned MG memberships in the literature and/or have BANYAN $\Sigma$  membership probabilities  $>10$  per cent, but that failed one or more of our kinematic tests (Section 4.4).

**04053103–0216257:** Although the DR2 parallax distance for this star is consistent with the range for the Hyades, this object is somewhat offset in from the cluster in sky position. It has a somewhat indeterminate BANYAN $\Sigma$  HYA membership probability of 48.9 per cent. Therefore, we tentatively assign it the status of a possible Hyades member.

**04181077+2317048:** The BANYAN $\Sigma$  membership probability for HYA is high (90.2 per cent), and there are several publications that recognize it as a member. Therefore, although it does not meet our kinematic criteria, it is a probable member of HYA.

**04500019+2229575:** The BANYAN $\Sigma$  probability is 99.7 per cent for TAU and its distance is consistent with TAU membership. Several publications claim its membership to TAU. The age based on Li EW is marginally consistent, so – although it does not meet our kinematic criteria – we concur that this star is a member of TAU.

**04524951–1955016:** This object has been assigned THA membership status in the literature, but broadly fails our kinematic criteria. Furthermore, it has an Li EW consistent with an age similar to that of the Pleiades. We suggest it is unlikely to be a THA member, and is instead a young field star.

**14590325–2406318:** BANYAN $\Sigma$  predicts a 94.6 per cent probability of membership with UCL. This object narrowly passes the  $\chi^2$  test and distance criterion for BPM, however the distance is far beyond the distance domain of BPM. Our MIKE spectrum for this object (see Fig. 3) reveals, for the first time, a strong Li EW line and thus we confirm this object as a highly likely member of UCL.

**22132028+8445372:** There is a 66.3 per cent probability of membership to ARG predicted by the BANYAN $\Sigma$  code. This object does not have any recorded RV and we could not find a

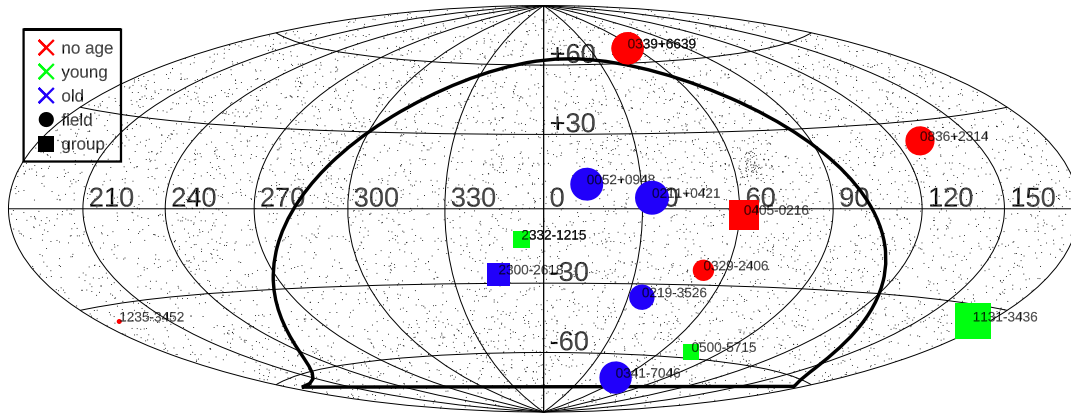


**Figure 10.** An Aitoff projection displaying the sky positions for the 14 CYS within 50 pc. Note that 0339+6639 comprises two stars in a resolved binary system. The colour scheme provides an age estimate for the stars based on assessment of Li EW, where objects in red lack any Li EW measurement therefore have an indeterminate age, blue symbols are objects that have no indication of youth, and green symbols are likely to be at least as young as the Pleiades. Square symbols indicate objects that belong to the potential MG member list in Table 6, even if they are suggested to be non-members in Section 5.1. Circles represent stars that have no entry in Table 6 and are very likely to be nearby field stars. The relative sizes of the symbols represent distance, with the closest stars appearing the largest. The small black dots on the plot represent  $\sim 6000$  K-stars within 50 pc identified in DR1 and the enclosed solid-black loop is the Galactic Plane.

corresponding RV value that would provide an  $\chi$ -squared match to ARG. There are no spectroscopic youth indicators for this object therefore we designated this for the present as a field star awaiting spectroscopic youth confirmation.

**23005681+3713528:** This object has a high ABD membership probability (97.5 per cent) from BANYAN $\Sigma$ , but narrowly fails the  $\chi^2$  test ( $=5.16$ ). It has previously been identified as a multiple system in the ABD MG, and we concur that it is most likely a member of ABD.

## 5.2 Stars within 50 pc not associated with MGs

There are 14 CYS stars within 50 pc. Almost all of these have been identified as members of multiple systems either from our duplicate RV analysis (see Section 4.2), from identifying apparently equidistant, comoving DR2 companions or from the source identification in Simbad. An Aitoff projection for the CYS within 50 pc is presented in Fig. 10, in equatorial coordinates, where the symbol sizes represent the distances (largest symbol, 20.3 pc, 11315526–3436272 and smallest symbol, 46.1 pc, 12353357–3452547) and small black filled circles represent the entire sample of K stars from the *Gaia* DR1 survey within 50 pc. Of the 14 CYS within 50 pc, nine are not listed in Table 6 and have no connection to nearby MGs; these are denoted with circles. Objects represented by squares are potential MG members (present in Table 6), even if they are subsequently rejected as members as a consequence of the analysis described in Section 5.1. 10 of the 14 CYS within 50 pc sample are located in the Southern hemisphere, yet none are found in the right ascension range  $190^\circ < \alpha < 330^\circ$ . This may reflect the avoidance of the Galactic plane in the GALEX survey. None of the 14 CYS within 50 pc that are possible MG members are identified in the Northern hemisphere.

Of the 14 CYS within 50 pc, only 8 stars have Li EW measurements from which ages might be inferred or constrained. Five of these eight stars have Li EWs that suggest they are at least older than the Pleiades. Four of these five are likely field objects, while one, 23005681+3713528, has a kinematic match with ABDMG, whose age is marginally older than the Pleiades;

indeed, the Li EW of 23005681+3713528 is consistent with that observed amongst similar ABDMG members. The other three stars have Li EWs that are consistent with the ages of clusters at least as young as the Pleiades. The Li EWs of these three stars match with stars of similar type in the MGs in which we have proposed membership (11315526–3436272 in TWA, 05004714–5715255 and 23323085–1215513 in BPMG; see Section 5.1).

Among the CYS within 50 pc, only 10 stars have counterparts in the RASS All-Sky-Survey, despite being presumably bright enough for detection. Of the stars with an RASS detection, only half have  $\log f_X/f_{\text{bol}} > -4.0$ , typical of K stars in young groups (see Section 3.3.2). Like the large  $f_X/f_{\text{bol}}$  spread of the Table 1 stars (Section 3.3.2), this suggests the CYSs include a significant number of apparently isochronally young stars ( $< 80$  Myr) that are UV-bright, but are weak X-ray emitters. We discuss the implications of this result in Section 6.

## 5.3 High probability young stars based on Li EW

In total, we identify five stars, at least as young as similar objects in the Pleiades, that are most likely to be young field stars. In Section 3.3.5, we identify 16 stars among the 146 CYS that have that have Li EW consistent with counterparts in the Pleiades or even younger groups. These are the objects in Table 3 (final column) with Li EW ages  $\leq 125$  Myr. We plot all stars with upper Li EW ages  $\leq 125$  Myr on an Aitoff projection in Fig. 11. The sample is presented in a similar manner to Fig. 10 in terms of age, distance, and group membership. There are 13 stars among these 16 that are present in Table 6 as potential MG members, although two of these, upon further assessment, 04524951–1955016 and 09503676–2933278 are more likely to be young field stars (Section 5.1). The three Li-rich stars that are not present in Table 6, 00092179+0038065, 06411248–5207385, and 22464298–1759072 are at least as young as 125 Myr and potentially form part of the nearby young field star population. Both 00092179+0038065 and 22464298–1759072 are listed in the original SACY sample, but have no MG membership assigned in the literature. The star 06411248–5207385 is suggested as a CAR member in Elliott et al. (2014), but we find zero probability

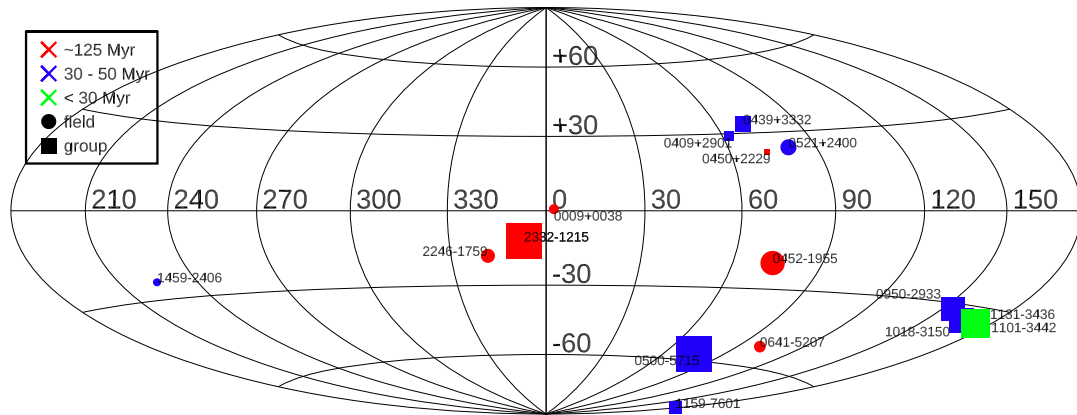


**Figure 11.** An Aitoff projection displaying the sky positions for the 16 stars that have Li EW upper ages  $\leq 125$  Myr.

of MG membership predicted by BANYAN $\Sigma$  for any MG and neither in any of our kinematic tests.

From the 39 stars with an Li EW measurement, our 16 stars with Li-based ages at least as young as the Pleiades give success rate in uncovering genuinely young stars of 40 per cent. It is possible that there remain a significant number of genuinely young field stars yet to be confirmed by their Li EW content. From the six stars for which we obtained spectra for the first time, we detected one star with strong Li absorption. We plot all stars with upper Li EW ages  $\leq 125$  Myr on an Aitoff projection in Fig. 11. The sample is presented in a similar manner to Fig. 10 in terms of age, distance, and group membership.

It is most likely that the majority of our CYS turn out to be unresolved binaries, and indeed, 30 per cent of the 146 CYS sample appear to be common proper motion binaries (see Section 4.2). Some of the earlier K-type stars match closely with a Pleiades binary sequence, and their multiplicity status could be identified by taking repeat spectroscopic observations to probe for variable RV profiles.

## 6 DISCUSSION

### 6.1 New and previously established MG members: a surprisingly low yield

We have identified 146 CYSs in our UV- and *Gaia*-DR1-based search for nearby ( $D \leq 120$  pc), isochronally young (age  $< 100$  Myr), low-mass ( $0.5\text{--}1.0M_{\odot}$ ) objects. The kinematics of our sample suggest that, despite their young isochronal ages, only  $\sim 10$  per cent belong to nearby MGs. Upon closer analysis, we find that 16 stars are possible or probable members of young, nearby groups. As shown in Table 6, out of our 23 candidate moving group members, two are members of the much older Hyades and five stars are likely to be part of the field population. Three possible or probable MG members have no previous literature assignment to any known MG, and the membership status of each of these remains tenuous, awaiting confirmation via additional spectroscopic indicators of youth and/or RV measurement. Based on rigorous kinematic analysis and age-dating assessments, we identify one new candidate member of OCT, 21351099+3402313, that shares similar *UVW* and is located at a suitable distance, but requires stronger evidence of youth for confirmation and another new, but weaker OCT candidate, 22233510+3402313, which requires both an RV measurement and further evidence of youth.

The fact that our CYS sample includes a handful of new MG candidates and more than a dozen previously identified nearby young stars, including the archetypical TW Hya, demonstrates the potential of our candidate selection criteria and follow-up kinematic test methods to identify such objects from among the field star population. Our yield of 16 young stars among 146 candidates (11 per cent) is comparable or better than those found in recent MG identification codes (Gagné et al. 2014; Riedel et al. 2017; Bowler et al. 2019; Schneider et al. 2019), where young star yields are generally far lower than 10 per cent. We note that there are 107 CYS that have no Li measurement as of yet, therefore our 11 per cent yield is a lower limit, and much likely to be higher given that the hit rate is  $\sim 40$  per cent amongst the 39 stars with Li measurements.

However, this yield still seems somewhat low, given that the sample of 146 was selected on the basis of *Gaia*-based isochronal ages  $\leq 80$  Myr (Fig. 1) as well as high levels of NUV excess (Fig. 5). Indeed, Figs 7 and 8 provide strong evidence that our sample of nearby young star candidates is in fact dominated by stars with ages older than the Pleiades, despite the fact that these stars lie high above the locus of MS stars in a *Gaia*/2MASS CMD (Fig. 1). From the sample of Li-rich objects in this work, we find five that are likely to be isolated, young field stars. Such objects may be extremely useful to examine the processes by which young stars, predominantly born in clusters, are ejected from their nascent groups and dissolve into the field star population and could provide a fuller picture of the kine-dynamical nature of young stellar population in the Solar vicinity.

There are 159 objects in Fig. 2 that were not included in our final CYS sample because either they had an insufficient number of visibility periods or failed the RUWE criteria (or both). Their positions on the DR2 CMD are not significantly different from the CYS sample, therefore we suspect that these other 159 objects are similarly ‘problematic’, in terms of their combination of (over)luminosities and UV excesses (i.e. looking young) on the one hand and demonstrating weak X-rays and anomalous kinematics (i.e. looking old) on the other. We expect that including these objects in our CYS sample would not alter the outcomes found in this study.

### 6.2 UV-bright and overluminous, but X-ray faint: a conundrum

As noted in Section 3.3.2, the CYS sample of 146 stars appears to be dominated by stars with rather low coronal activity levels, based on their low overall RASS X-ray detection rate as well as the

low X-ray fluxes of many of the individual stars that were detected. More specifically, the majority of the RASS-detected stars lie within  $\sim 75$  pc (Fig. 7), despite the fact that the RASS was capable of detecting K and early-M-type stars of Pleiades or younger age out to  $\sim 100$  pc (e.g. Rodriguez et al. 2013, their fig. 15 and table 6). The weak X-ray fluxes of a majority of the CYS sample is also reflected in the fact that 5 of the 14 stars within 50 pc have  $\log L_X/L_{\text{bol}} < -4.0$ , and another four were undetected in the RASS, suggesting even lower relative X-ray luminosities. That such a large fraction of the CYS sample display low coronal activity levels is surprising, given that all stars were selected on the basis of GALEX UV detections and young ( $\leq 80$  Myr) isochronal ages. These results could have far-reaching implications for the use of *Gaia*-based isochronal ages to select CYSs for purposes of testing models of the manifestation and evolution of stellar magnetic activity (see e.g. fig. 5 in Zari et al. 2018).

We can likely rule out the following five potential explanations for the non-young-star-like X-ray and kinematic properties of the majority of the candidates:

(i) Contamination by first-ascent giant stars. This explanation would appear to be at odds both with the CMD distribution of the candidates (Fig. 1) and with the frequency of UV excesses among the candidate stars (Fig. 5). Our spectroscopic observations (Section 3.1) also yielded no evidence of contamination of the CYS sample by giants.

(ii) Binaries with a narrow range of separations. Binary stars with separations such that both stars are included in 2MASS photometry ( $\sim 2$  arcsec PSF), but only the primary is measured by *Gaia* at  $G$  band, would shift an apparently single star upwards and to the right in Fig. 1. However, such confusion should only apply to a highly specific subsample of binary stars with separations around  $\sim 1$  arcsec which are likely to have been detected in DR2 (see Section 4.2), and there appears to be very little effect on the CMD when plotted using purely DR2 photometry (Fig. 12).

(iii) Higher order multiple systems. It would take *at least* an equal-mass quadruple system for a typical multiple MS system to appear even close to the locus of our CYSs. The rate of occurrence for higher order multiples ( $N \geq 4$ ) is  $\sim 3$  per cent (Raghavan et al. 2010), and these should have been resolved by DR2 in any case. Therefore, we rule out the higher order multiple hypothesis.

(iv) MS stars with white dwarf (WD) companions. A subset of our candidates may be MS stars that have been spun-up and/or inflated by accretion of mass lost by the asymptotic giant branch antecedent of a companion WD (Jeffries & Stevens 1996), such that the WD is in fact a contributor to (or dominates) the UV detected by GALEX. But it seems highly improbable that such systems would dominate our sample.

(v) Super metal-rich ( $[\text{Fe}/\text{H}] > 0.2$ ) stars. Although very rare, the most extreme known metal-rich stars have  $[\text{Fe}/\text{H}] \sim 0.3$  dex (Feltzing & Gonzalez 2001), and stars with higher metallicities have larger luminosities. In Fig. 12 we plot an 80 Myr (PARSEC 3.1) isochrone at this metallicity; it is apparent that the CYS sample stars are much brighter than this isochrone. A combination of both high metallicity and multiplicity may in some cases place MS stars close to the locus of our CYS sample. However, it is exceedingly unlikely that a significant number of our CYSs are in this category.

In the absence of a better explanation, the surprising ‘bifurcation’ of our UV- and isochronally selected nearby young star candidates into X-ray-bright and X-ray-faint subsamples (Section 3.3.2; Fig. 7) raises a set of particularly vexing questions. Namely: if the large (apparently dominant) fraction of X-ray faint stars among our

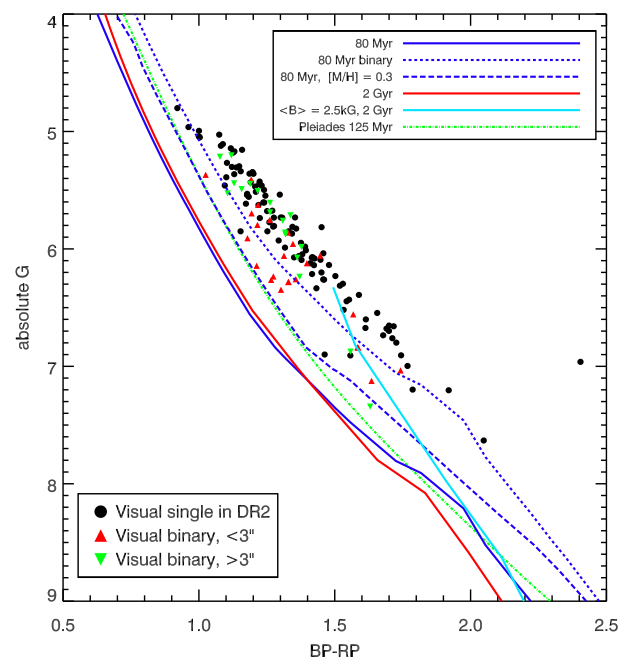


**Figure 12.** The same absolute  $G$  versus  $G_{\text{BP}} - G_{\text{RP}}$  CMD as in Fig. 2 for the CYS sample, where visual single stars are displayed as black filled circles, close visual binaries as red upwards-facing triangles, and wide visual binaries as green downwards-facing triangles (see Section 4.2). The wide-dashed blue line represents an 80 Myr with  $[\text{Fe}/\text{H}] = 0.3$  dex and the solid cyan line describes a 2 Gyr isochrone with surface magnetic fields  $\langle B \rangle = 2.5$  kG (Feiden 2016, see Section 6).

candidates are in fact not pre-MS stars, then why are they as ‘overluminous’ (in terms of their bolometric luminosities) as the X-ray-bright stars?

Could (at least some of) our sample be ‘imposters’ – zero-age (or even older) MS stars that are ‘puffed up’ via high levels of magnetic activity due to fast rotation rates, as appears to be the case for, e.g. the subset of overluminous late-type Pleiades stars (Somers & Stassun 2017)? We compare our CYS sample with a 2 Gyr single-star isochrone from the Dartmouth evolutionary models, with strong surface magnetic fields (Feiden 2016,  $\langle B \rangle = 2.5$  kG), since strong magnetic fields are expected to inflate radii of K/M-type stars thus increasing their bolometric luminosities (Somers & Stassun 2017; Jackson, Deliyannis & Jeffries 2018).<sup>6</sup> The magnetic models only go as massive as  $M/M_{\odot} = 0.8$ , however we can still identify that the low-mass stars (early K-type and beyond) generally lie above the magnetic MS, however some of the sample lie within the bounds of the magnetic models. It is within reason that MS stars with large magnetic fields could partially explain overluminosity (with  $\langle B \rangle = 2.5$  kG, see Fig. 12), however older stars are highly unlikely to be so strongly magnetically active (for example, Folsom et al. 2018, find no early MS Solar-type stars with surface magnetic fields  $> 0.2$  kG), and in any case, if they have strong magnetic fields they should have been supported by evidence of activity, e.g. strong  $H\alpha$  emission, which we do not observe for the vast majority of our CYS sample.

It is furthermore possible that these apparently overluminous stars manifest significant photometric variability. If this variability

<sup>6</sup>The outputs from the magnetic models give  $\log L$  and  $\log T_{\text{eff}}$ , so we use the EEM table to obtain the appropriate  $G_{\text{BP}} - G_{\text{RP}}$  and  $M_G$  values.

were at levels of a few tenths of a magnitude, they might transiently appear more luminous than their non-variable (older) counterparts. There are 80 sources in our CYS that have SuperWASP identifiers within 10 arcsec and more than 1000 photometric data points. All but six of these have both standard deviations and 5–95th percentile ranges less than 0.2 mag, and the other six appear to have large photometric errors. Even if these stars did demonstrate high levels of photometric variability, why do so many of our magnetically active, presumably radially inflated young MS field stars have such weak coronae relative to ‘normal’ young stars, despite their apparently similar levels of chromospheric UV excess?

Could some or all of these stars be rotationally inflated yet X-ray faint due to centrifugally induced ‘coronal stripping’ (Jardine 2004)? This is highly unlikely as it would apply to ultrafast rotating stars that are supersaturated in X-ray. These are only slightly less X-ray active than the ‘saturated’ X-ray emitters ( $\log L_X/L_{\text{bol}} \sim -3$ ), and would have periods of  $\leq 0.5$  d (and would still be very spotted, and very active). Such stars would have stood out in X-ray surveys and many would have been previously found as active stars with measured rotation periods due to spottedness. Such characteristics are notably lacking for most of the CYS sample.

Addressing these questions will require a dedicated observing campaign targeting our candidate stars in the optical through UV to X-ray regimes, so as to access diagnostics of chromospheric and coronal activity and relate these properties to stellar age indicators and rotation rates. Ultraviolet spectroscopy with *HST*, as well as *Chandra* and *XMM* X-ray spectroscopy, represent the additional, essential puzzle pieces necessary to understand the natures of the class of isochronally young and UV-bright yet X-ray faint and kinematically ‘old’ stars uncovered by this work. Regardless, the work presented here, like that of Wright & Mamajek (2018), hints at the power of *Gaia* astrometric and photometric data for purposes of isolating the population of young MS stars that originated in young moving groups and have relatively recently mixed into the field star population.

## 7 SUMMARY AND CONCLUSIONS

We have identified a kinematically and almost spatially unbiased sample of 146 nearby, isochronally young, UV-excessive K-type stars, and we conduct astrometric and age-dating analyses to identify their astrophysical nature. We find only  $\sim 10$  per cent of the sample can be classed as highly likely young stars and in most cases one must find alternative scenarios to explain their overluminosity compared to typical MS counterparts. A small, but presumably representative spectroscopic sample uncovered just one new young star. This spectroscopic sample provided a useful supplement for measuring Galactic kinematics.

About three-quarters of the full sample of 146 stars have sufficient data to measure Galactic space velocities. We identify 16 of these stars that satisfy kinematic criteria for membership to at least one nearby MG. Five are new candidate members with no previous identification of MG membership. There are five stars with Li EW measurements consistent with age upper limits of  $\sim 125$  Myr which appear to be isolated, young, nearby field stars.

Puzzlingly, a significant fraction of the UV-bright, overluminous stars here identified as CYSs either do not have X-ray detections or have very low X-ray activity, despite being close enough ( $D \leq 50$  pc) to surpass X-ray sensitivity limits. These objects, whether young or more evolved, appear to pose significant challenges to our present understanding of magnetic activity in late-type stars. Additional UV and X-ray spectroscopic observations are required

to ascertain the natures of these overluminous, UV-bright, yet X-ray-weak stars.

Finally, we reiterate (see Section 2) that the same selection criteria used to isolate the 146 stars in Table 1 from *Gaia* DR1 data would yield in excess of 1500 candidate stars, if applied to DR2 data. In addition to yielding a larger number of new candidate MG members, investigation of this DR2 ‘supersample’ would likely yield greater insight into the puzzling UV versus X-ray behaviours of overluminous field stars.

## ACKNOWLEDGEMENTS

ASB acknowledges the financial support of the STFC and UNAM. This research was supported by NASA Astrophysics Data Analysis Program (ADAP) grant NNX12AH37G to RIT and UCLA and NASA ADAP grant NNX09AC96G to RIT, and by a National Science Foundation Research Experience for Undergraduates program grant to RIT’s Center for Imaging Science that supported M. Chalifour’s summer 2017 RIT residency. The authors thank R. Jeffries for helpful discussions. The authors thank the anonymous referees for useful suggestions and comments, which have significantly improved this manuscript.

## REFERENCES

- Alonso-Floriano F. J. et al., 2015, *A&A*, 577, A128  
 Ansdell M. et al., 2015, *ApJ*, 798, 41  
 Baraffe I., Homeier D., Allard F., Chabrier G., 2015, *A&A*, 577, A42  
 Barbier-Brossat M., Petit M., Figon P., 1994, *A&AS*, 108, 603  
 Barenfeld S. A., Bubar E. J., Mamajek E. E., Young P. A., 2013, *ApJ*, 766, 6  
 Bell C. P. M., Mamajek E. E., Naylor T., 2015, *MNRAS*, 454, 593  
 Bell C. P. M., Murphy S. J., Mamajek E. E., 2017, *MNRAS*, 468, 1198  
 Bernstein R., Sheckman S. A., Gunnels S. M., Mochnacki S., Athey A. E., 2003, in Iye M., Moorwood A. F. M., eds, Proc. SPIE Conf. Ser. Vol. 4841, Instrument Design and Performance for Optical/Infrared Ground-based Telescopes. SPIE, Bellingham, p. 1694  
 Bianchi L., 2014, *ApSS*, 354, 103  
 Binks A. S., Jeffries R. D., 2014, *MNRAS*, 438, L11  
 Binks A. S., Jeffries R. D., 2017, *MNRAS*, 469, 579  
 Binks A. S., Jeffries R. D., Maxted P. F. L., 2015, *MNRAS*, 452, 173  
 Binks A. S., Jeffries R. D., Ward J. L., 2018, *MNRAS*, 473, 2465  
 Boller T., Freyberg M. J., Trümper J., Haberl F., Voges W., Nandra K., 2016, *A&A*, 588, A103  
 Bouvier J. et al., 2018, *A&A*, 613, A63  
 Bowler B. P., Liu M. C., Shkolnik E. L., Tamura M., 2015, *ApJS*, 216, 7  
 Bowler B. P. et al., 2019, *ApJ*, 877, 60  
 Bressan A., Marigo P., Girardi L., Salasnich B., Dal Cero C., Rubele S., Nanni A., 2012, *MNRAS*, 427, 127  
 Cayrel de Strobel G., Spite M., 1988, in Cayrel de Strobel G., Spite M., eds, Proc. IAU Symp. 132, The Impact of Very High S/N Spectroscopy on Stellar Physics. Kluwer, Dordrecht, p. 449  
 Chauvin G. et al., 2015, *A&A*, 573, A127  
 Coelho P., Barbuy B., Meléndez J., Schiavon R. P., Castilho B. V., 2005, *A&A*, 443, 735  
 Cummings J. D., Deliyannis C. P., Maderak R. M., Steinhauer A., 2017, *AJ*, 153, 128  
 da Silva L., Torres C. A. O., de La Reza R., Quast G. R., Melo C. H. F., Sterzik M. F., 2009, *A&A*, 508, 833  
 De Silva G. M., D’Orazi V., Melo C., Torres C. A. O., Gieles M., Quast G. R., Sterzik M., 2013, *MNRAS*, 431, 1005  
 Dent W. R. F. et al., 2013, *PASP*, 125, 477  
 Dopita M., Hart J., McGregor P., Oates P., Bloxham G., Jones D., 2007, *Ap&SS*, 310, 255  
 Duflo M., Figon P., Meyssonnier N., 1995, *A&AS*, 114, 269

- Elliott P., Bayo A., Melo C. H. F., Torres C. A. O., Sterzik M., Quast G. R., 2014, *A&A*, 568, A26
- Fang M. et al., 2017, *AJ*, 153, 188
- Feiden G. A., 2016, *A&A*, 593, A99
- Feltzing S., Gonzalez G., 2001, *A&A*, 367, 253
- Fernández D., Figueras F., Torra J., 2008, *A&A*, 480, 735
- Folsom C. P. et al., 2018, *MNRAS*, 474, 4956
- Frasca A., Montes D., Alcalá J. M., Klutsch A., Guillout P., 2018, *Acta Astron.*, 68, 403
- Gagné J., Lafrenière D., Doyon R., Malo L., Artigau É., 2014, *ApJ*, 783, 121
- Gagné J. et al., 2018, *ApJ*, 856, 23
- Gaia Collaboration, 2016, *A&A*, 595, A2
- Gaia Collaboration, 2018, *A&A*, 616, A1
- Gaidos E. et al., 2014, *MNRAS*, 443, 2561
- Gliese W., Jahreiss H., 1991, NASA STI/Recon Technical Report A, 92, 33932
- Gontcharov G. A., 2006, *Astron. Astrophys. Trans.*, 25, 145
- Guenther E. W., Esposito M., Mundt R., Covino E., Alcalá J. M., Cusano F., Stecklum B., 2007, *A&A*, 467, 1147
- Hawley S. L., Reid I. N., Gizis J. E., Byrne P. B., 1999, in Butler C. J., Doyle J. G., eds, ASP Conf. Ser. Vol. 158, Solar and Stellar Activity: Similarities and Differences. Astron. Soc. Pac., San Francisco, p. 63
- Hernandez J., Briceño C., Calvet N., Hartmann L., Berlind P., Luhman K., 2017, Astrophysics Source Code Library, record ascl:1705.005
- Hughes A. M., Duchêne G., Matthews B. C., 2018, *ARA&A*, 56, 541
- Jackson R. J., Deliyannis C. P., Jeffries R. D., 2018, *MNRAS*, 476, 3245
- Jardine M., 2004, *A&A*, 414, L5
- Jeffries R. D., 2014, in Lebreton Y., Valls-Gabaud D., Charbonnel C., eds, EAS Publ. Ser. Vol. 65, The Ages of Stars. Cambridge Univ. Press, Cambridge, p. 289
- Jeffries R. D., Oliveira J. M., 2005, *MNRAS*, 358, 13
- Jeffries R. D., Stevens I. R., 1996, *MNRAS*, 279, 180
- Johnson D. R. H., Soderblom D. R., 1987, *AJ*, 93, 864
- Kalas P., 2004, American Astronomical Society Meeting Abstracts #204. p. 690
- Kastner J. H., 2016, in Kastner J. H., Stelzer B., Metchev S. A., eds, Proc. IAU Symp. 314, Young Stars & Planets Near the Sun. Kluwer, Dordrecht, p. 16
- Kastner J. H., 2018, *Res. Notes Am. Astron. Soc.*, 2, 137
- Kastner J. H., Zuckerman B., Weintraub D. A., Forveille T., 1997, *Science*, 277, 67
- Kastner J. H., Principe D. A., Punzi K., Stelzer B., Gorti U., Pascucci I., Argiroffi C., 2016, *AJ*, 152, 3
- Kastner J. H., Sacco G., Rodriguez D., Punzi K., Zuckerman B., Vican Haney L., 2017, *ApJ*, 841, 73
- Kraus A. L., Herczeg G. J., Rizzuto A. C., Mann A. W., Slesnick C. L., Carpenter J. M., Hillenbrand L. A., Mamajek E. E., 2017, *ApJ*, 838, 150
- Kunder A. et al., 2017, *AJ*, 153, 75
- Lagrange A.-M. et al., 2009, *A&A*, 493, L21
- Lawler S. M. et al., 2009, *ApJ*, 705, 89
- Lindegren L., 2018, Re-normalising the astrometric chisquare in Gaia DR2. Technical note GAIA-C3-TB-LU-LL124-01, Gaia Data Processing and Analysis Consortium
- Li J. Z., Hu J. Y., 1998, *A&AS*, 132, 173
- Luo A.-L. et al., 2015, *Research in Astronomy and Astrophysics*, 15, 1095
- MacGregor M. A., Wilner D. J., Andrews S. M., Hughes A. M., 2015, *ApJ*, 801, 59
- Malaroda S. et al., 2000, *A&AS*, 144, 1
- Malo L., Doyon R., Lafrenière D., Artigau É., Gagné J., Baron F., Riedel A., 2013, *ApJ*, 762, 88
- Malo L., Artigau É., Doyon R., Lafrenière D., Albert L., Gagné J., 2014a, *ApJ*, 788, 81
- Malo L., Doyon R., Feiden G. A., Albert L., Lafrenière D., Artigau É., Gagné J., Riedel A., 2014b, *ApJ*, 792, 37
- Mamajek E. E., 2016, in Kastner J. H., Stelzer B., Metchev S. A., eds, Proc. IAU Symp. 314, Young Stars & Planets Near the Sun. Kluwer, Dordrecht, p. 21
- Mamajek E. E., Bell C. P. M., 2014, *MNRAS*, 445, 2169
- Mamajek E. E., Lawson W. A., Feigelson E. D., 2000, *ApJ*, 544, 356
- Martín E. L., Lodieu N., Pavlenko Y., Béjar V. J. S., 2018, *ApJ*, 856, 40
- Matthews B. C., Krivov A. V., Wyatt M. C., Bryden G., Eiroa C., 2014, in Beuther H., Klessen R. S., Dullemond C. P., Henning T., eds, Protostars and Planets VI. Univ. Arizona Press, Tucson, AZ, p. 521
- Melis C., Reid M. J., Mioduszewski A. J., Stauffer J. R., Bower G. C., 2014, *Science*, 345, 1029
- Mentuch E., Brandeker A., van Kerkwijk M. H., Jayawardhana R., Hauschildt P. H., 2008, *ApJ*, 689, 1127
- Messina S. et al., 2016, *A&A*, 596, A29
- Montes D., López-Santiago J., Fernández-Figueroa M. J., Gálvez M. C., 2001, *A&A*, 379, 976
- Murphy S. J., Lawson W. A., Bessell M. S., 2013, *MNRAS*, 435, 1325
- Nguyen D. C., Brandeker A., van Kerkwijk M. H., Jayawardhana R., 2012, *ApJ*, 745, 119
- Olivares J. et al., 2018, *A&A*, 617, A15
- Pecaut M. J., Mamajek E. E., 2013, *ApJS*, 208, 9
- Prisinzano L., Micela G., Sciortino S., Affer L., Damiani F., 2012, *A&A*, 546, A9
- Prisinzano L. et al., 2016, *A&A*, 589, A70
- Raghavan D. et al., 2010, *ApJS*, 190, 1
- Reid N., Hawley S. L., Mateo M., 1995, *MNRAS*, 272, 828
- Rhee J. H., Song I., Zuckerman B., 2007, *ApJ*, 671, 616
- Riaz B., Gizis J. E., Harvin J., 2006, *AJ*, 132, 866
- Riedel A. R., Blunt S. C., Lambrides E. L., Rice E. L., Cruz K. L., Faherty J. K., 2017, *AJ*, 153, 95
- Riedel A. R., Silverstein M. L., Henry T. J., Jao W.-C., Winters J. G., Subasavage J. P., Malo L., Hambly N. C., 2018, *AJ*, 156, 49
- Rodriguez D. R., Zuckerman B., Kastner J. H., Bessell M. S., Faherty J. K., Murphy S. J., 2013, *ApJ*, 774, 101
- Schlieder J. E., Lépine S., Simon M., 2010, *AJ*, 140, 119
- Schlieder J. E., Lépine S., Simon M., 2012, *AJ*, 144, 109
- Schneider A., Melis C., Song I., 2012, *ApJ*, 754, 39
- Schneider A. C., Shkolnik E. L., Allers K. N., Kraus A. L., Liu M. C., Weinberger A. J., Flagg L., 2019, *AJ*, 157, 234
- Shkolnik E. L., Liu M. C., Reid I. N., Dupuy T., Weinberger A. J., 2011, *ApJ*, 727, 6
- Soderblom D. R., Pilachowski C. A., Fedele S. B., Jones B. F., 1993, *AJ*, 105, 2299
- Somers G., Stassun K. G., 2017, *AJ*, 153, 101
- Sperauskas J., Bartašiūtė S., Boyle R. P., Deveikis V., Raudeliūnas S., Upgren A. R., 2016, *A&A*, 596, A116
- Stauffer J. R., Schultz G., Kirkpatrick J. D., 1998, *ApJ*, 499, L199
- Stelzer B., Marino A., Micela G., López-Santiago J., Liefke C., 2013, *MNRAS*, 431, 2063
- Tognelli E., Prada Moroni P. G., Degl'Innocenti S., 2011, *A&A*, 533, A109 (T11)
- Tonry J., Davis M., 1979, *AJ*, 84, 1511
- Torres C. A. O., Quast G. R., da Silva L., de La Reza R., Melo C. H. F., Sterzik M., 2006, *A&A*, 460, 695
- Torres C. A. O., Quast G. R., Melo C. H. F., Sterzik M. F., 2008, in Reipurth B., ed., Handbook of Star Forming Regions, Volume II: The Southern Sky ASP Monograph Publications, Vol. 5. Astron. Soc. Pac., San Francisco, p. 757
- Voges W. et al., 1999, *A&A*, 349, 389
- Voges W. et al., 2000, *IAU Circ.*, 7432, 3
- Wahhaj Z. et al., 2010, *ApJ*, 724, 835
- Watson C. L., Henden A. A., Price A., 2006, in Warner B. et al., eds, The Society for Astronomical Sciences 25th Annual Symposium on Telescope Science. Soc. Astron. Sci., Big Bear, California, p. 47
- Wenger M. et al., 2000, *A&AS*, 143, 9
- White R. J., Basri G., 2003, *ApJ*, 582, 1109
- White R. J., Gabor J. M., Hillenbrand L. A., 2007, *AJ*, 133, 2524
- Wichmann R. et al., 1996, *A&A*, 312, 439
- Wichmann R. et al., 2000, *A&A*, 359, 181
- Winters J. G. et al., 2019, *AJ*, 157, 216

- Wright N. J., Mamajek E. E., 2018, *MNRAS*, 476, 381  
Wyatt M. C., 2008, *ARA&A*, 46, 339  
Yee J. C., Jensen E. L. N., 2010, *ApJ*, 711, 303  
Zari E., Hashemi H., Brown A. G. A., Jardine K., de Zeeuw P. T., 2018, *A&A*, 620, A172  
Žerjal M. et al., 2017, *ApJ*, 835, 61  
Zuckerman B., Song I., 2004, *ARA&A*, 42, 685

## SUPPORTING INFORMATION

Supplementary data are available at *MNRAS* online.

**Table 1.** The 2MASS identifier names, spectral types based on linear interpolation of  $G - K_s$  colour (SpTp), spectral types given in SIMBAD (SpTs), *Galex* NUV magnitudes, DR2 photometry, 2MASS K magnitudes, X-ray to bolometric luminosities, and UV excesses for the candidate young stars.

**Table 4.** Stars with probable common proper motion companions in DR2, where column 2 describes the angular separation between the components.

**Table 5.** Kinematic data for the candidate young stars.

Please note: Oxford University Press is not responsible for the content or functionality of any supporting materials supplied by the authors. Any queries (other than missing material) should be directed to the corresponding author for the article.

This paper has been typeset from a  $\text{\TeX/L\TeX}$  file prepared by the author.